Computational Predictions of Epitaxy and Substrate-Directed Nucleation

Brian K. Olmsted and Michael D. Ward

Contribution from the Molecular Design Institute, Department of Chemistry, New York University, 100 Washington Square East, New York, NY 10003-6688

Supporting Information

Contents in the Supporting Information:

- Figures **S1** to **S20**: GRACE Calculations for epitaxy
- Figures **S21** to **S44**: X-ray Microdiffraction data
- Table **S1**: Crystallographic data for polymorphic compounds studied
- Table **S2**: Lattice parameters for substrates studied
- Download GRACE at: http://www.nyu.edu/fas/dept/chemistry/wardgroup/Software.html
- Figure **S45**: Enlargement of **Figure 5** from the manuscript.

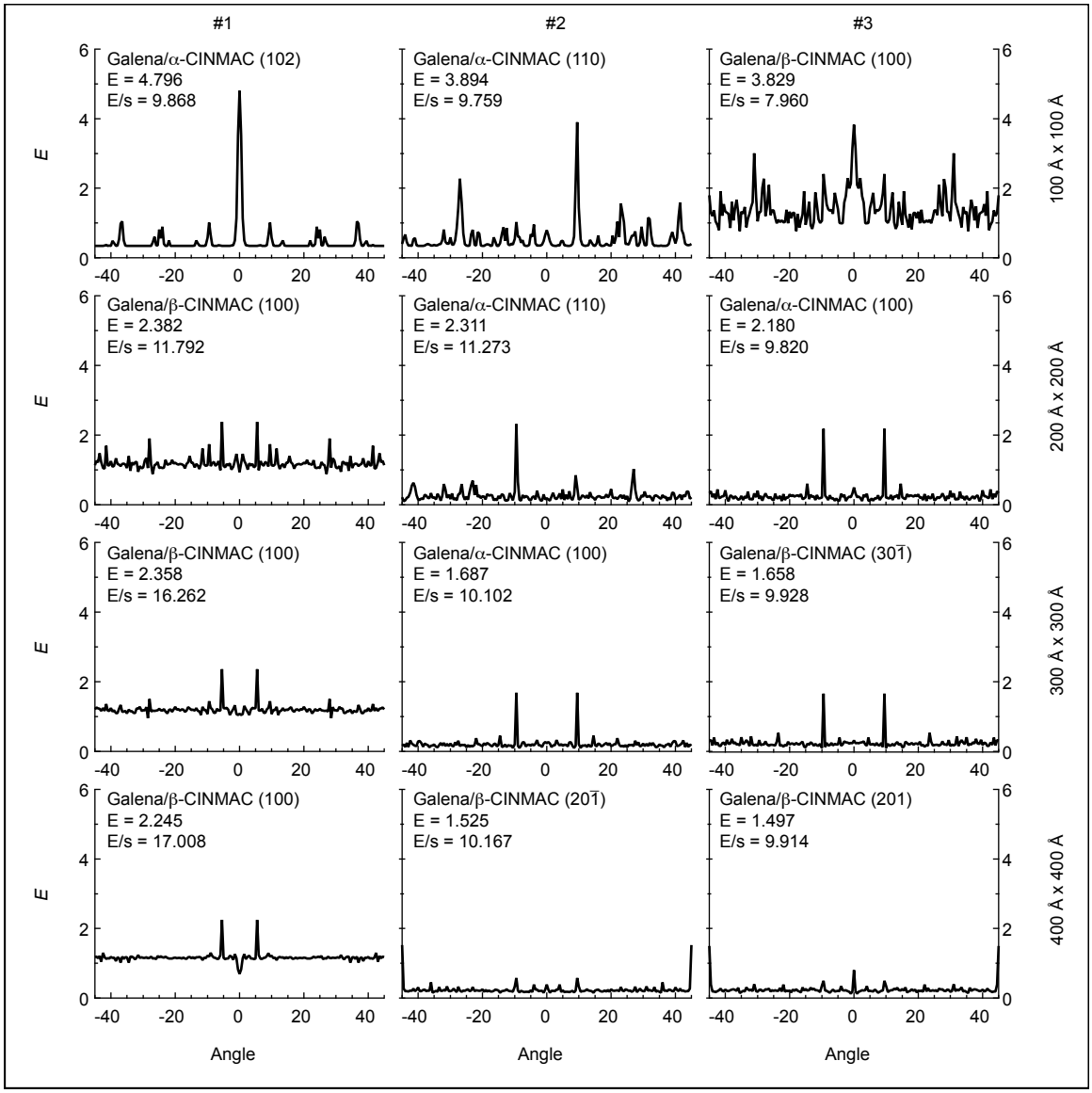

Figure S1. GRACE calculations for *trans*-cinnamic acid and galena in terms of epitaxy score (*E*) versus azimuthal angle between the substrate lattice and the overlayer lattice. Columns are ordered from left to right with respect to the first, second, and third best epitaxy score. Rows are ordered from top to bottom with respect to area of calculation.

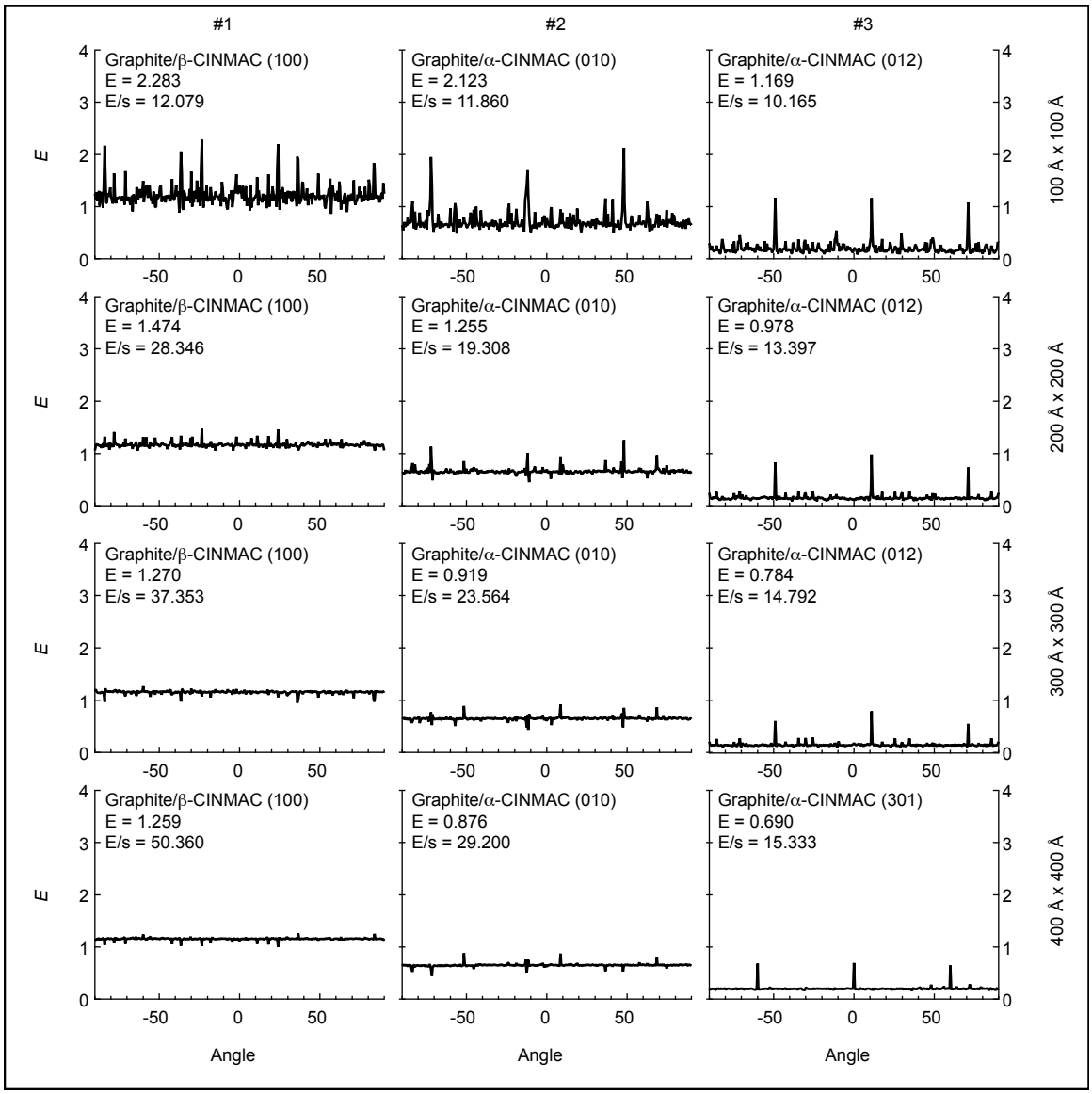

Figure S2. GRACE calculations for *trans*-cinnamic acid and HOPG in terms of epitaxy score (*E*) versus azimuthal angle between the substrate lattice and the overlayer lattice. Columns are ordered from left to right with respect to the first, second, and third best epitaxy score. Rows are ordered from top to bottom with respect to area of calculation.

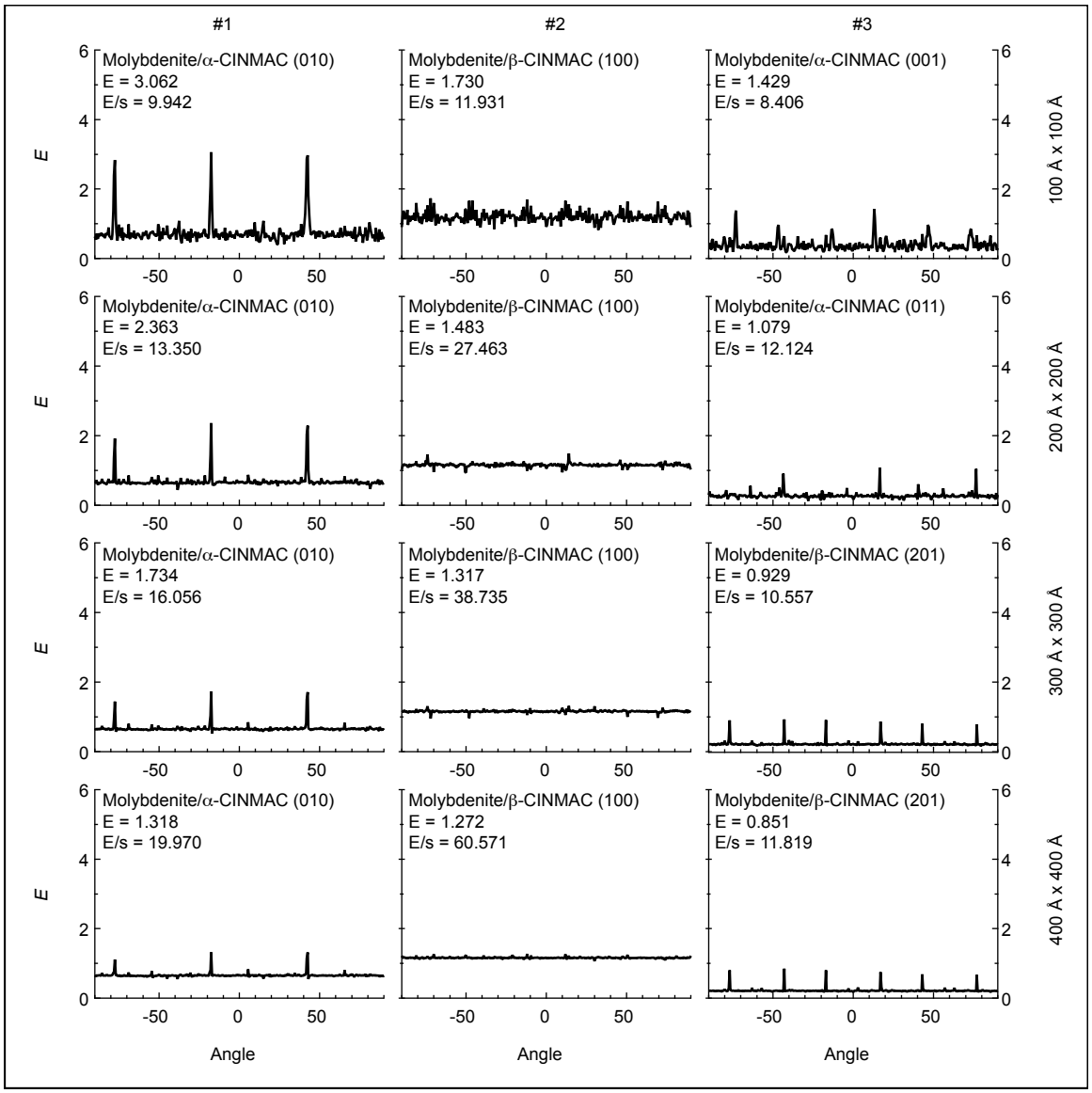

Figure S3. GRACE calculations for *trans*-cinnamic acid and molybdenite in terms of epitaxy score (*E*) versus azimuthal angle between the substrate lattice and the overlayer lattice. Columns are ordered from left to right with respect to the first, second, and third best epitaxy score. Rows are ordered from top to bottom with respect to area of calculation.

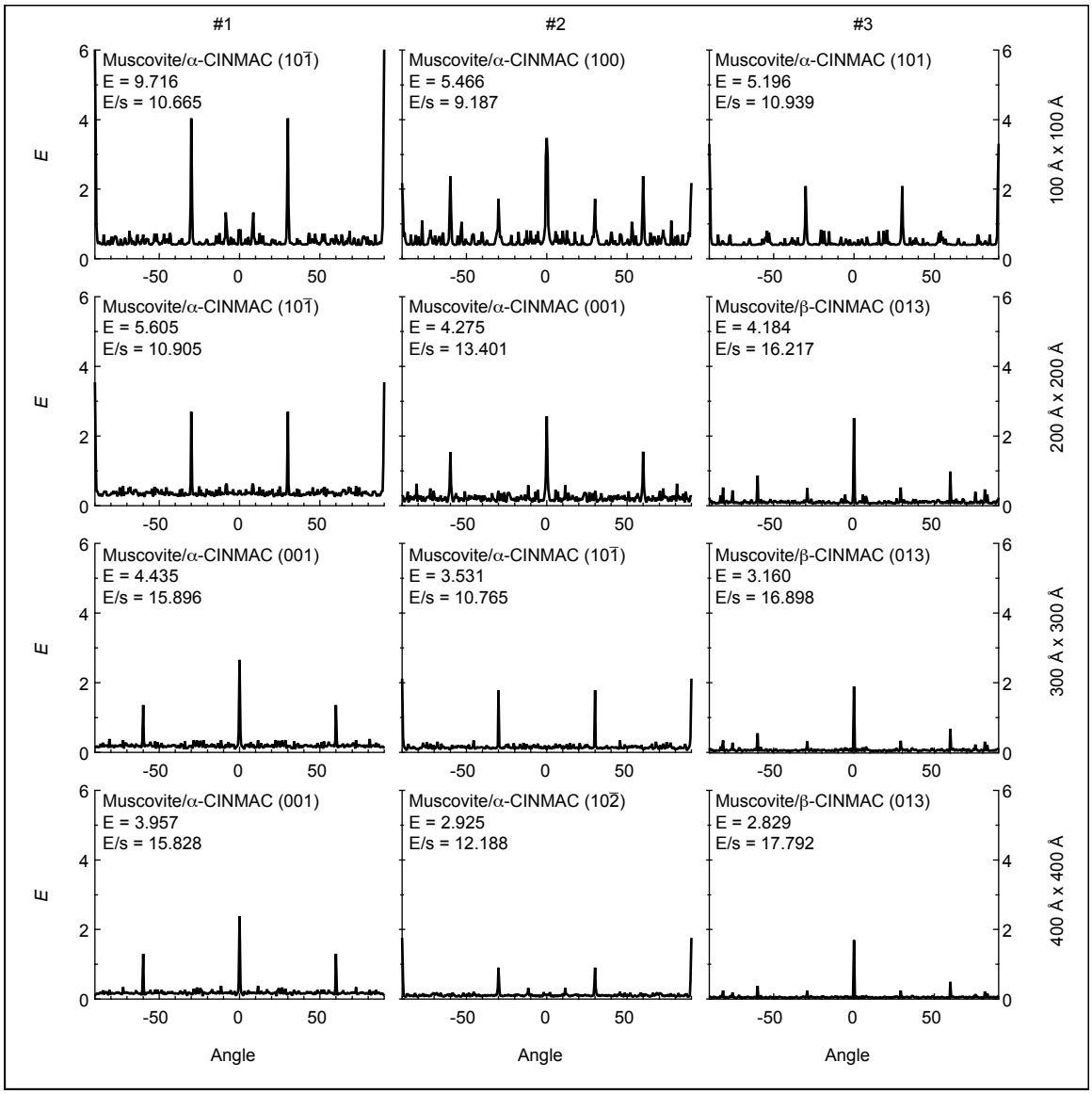

Figure S4. GRACE calculations for *trans*-cinnamic acid and muscovite in terms of epitaxy score (*E*) versus azimuthal angle between the substrate lattice and the overlayer lattice. Columns are ordered from left to right with respect to the first, second, and third best epitaxy score. Rows are ordered from top to bottom with respect to area of calculation.

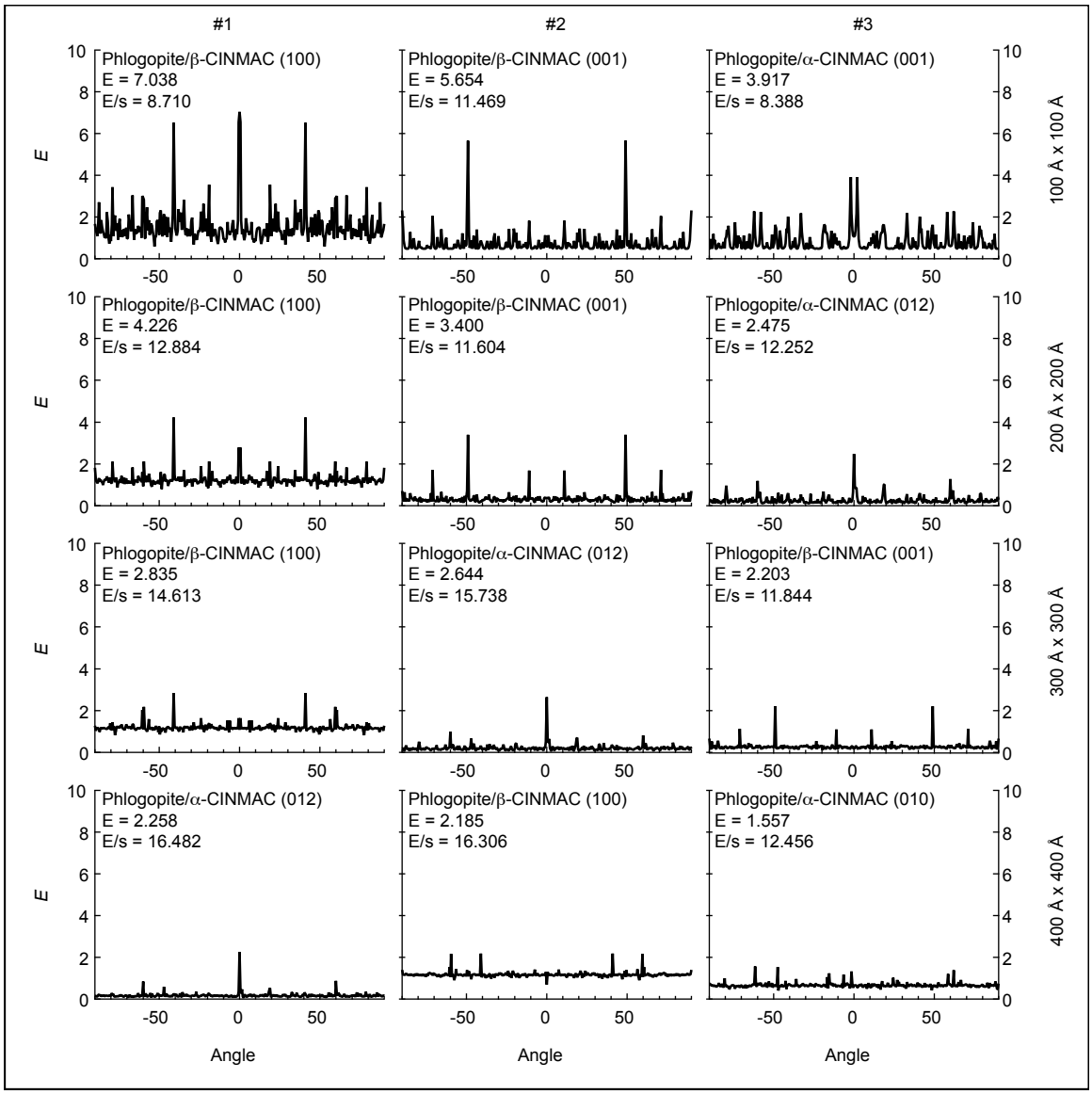

Figure S5. GRACE calculations for *trans*-cinnamic acid and phlogopite in terms of epitaxy score (*E*) versus azimuthal angle between the substrate lattice and the overlayer lattice. Columns are ordered from left to right with respect to the first, second, and third best epitaxy score. Rows are ordered from top to bottom with respect to area of calculation.

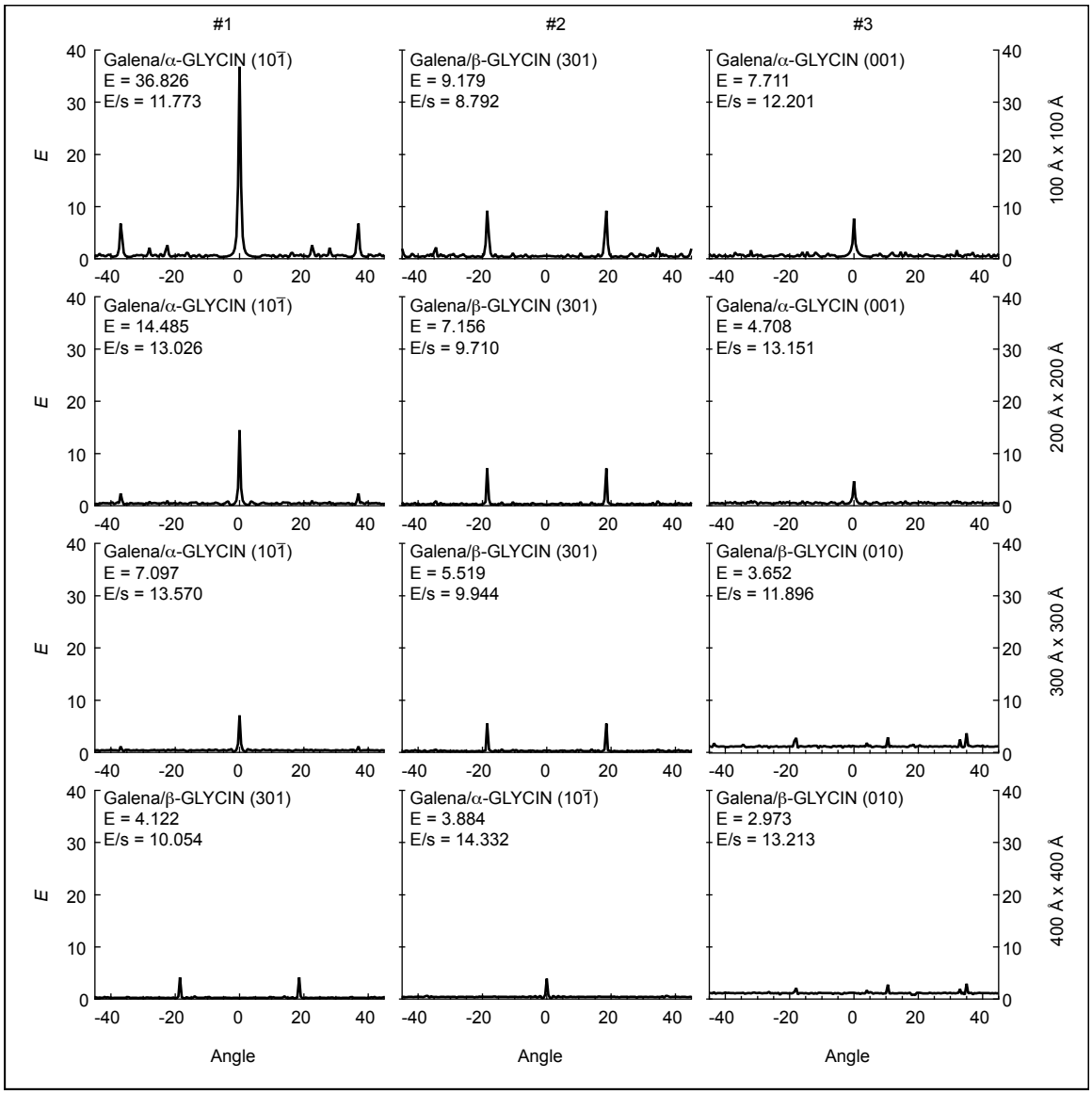

Figure S6. GRACE calculations for glycine and galena in terms of epitaxy score (*E*) versus azimuthal angle between the substrate lattice and the overlayer lattice. Columns are ordered from left to right with respect to the first, second, and third best epitaxy score. Rows are ordered from top to bottom with respect to area of calculation.

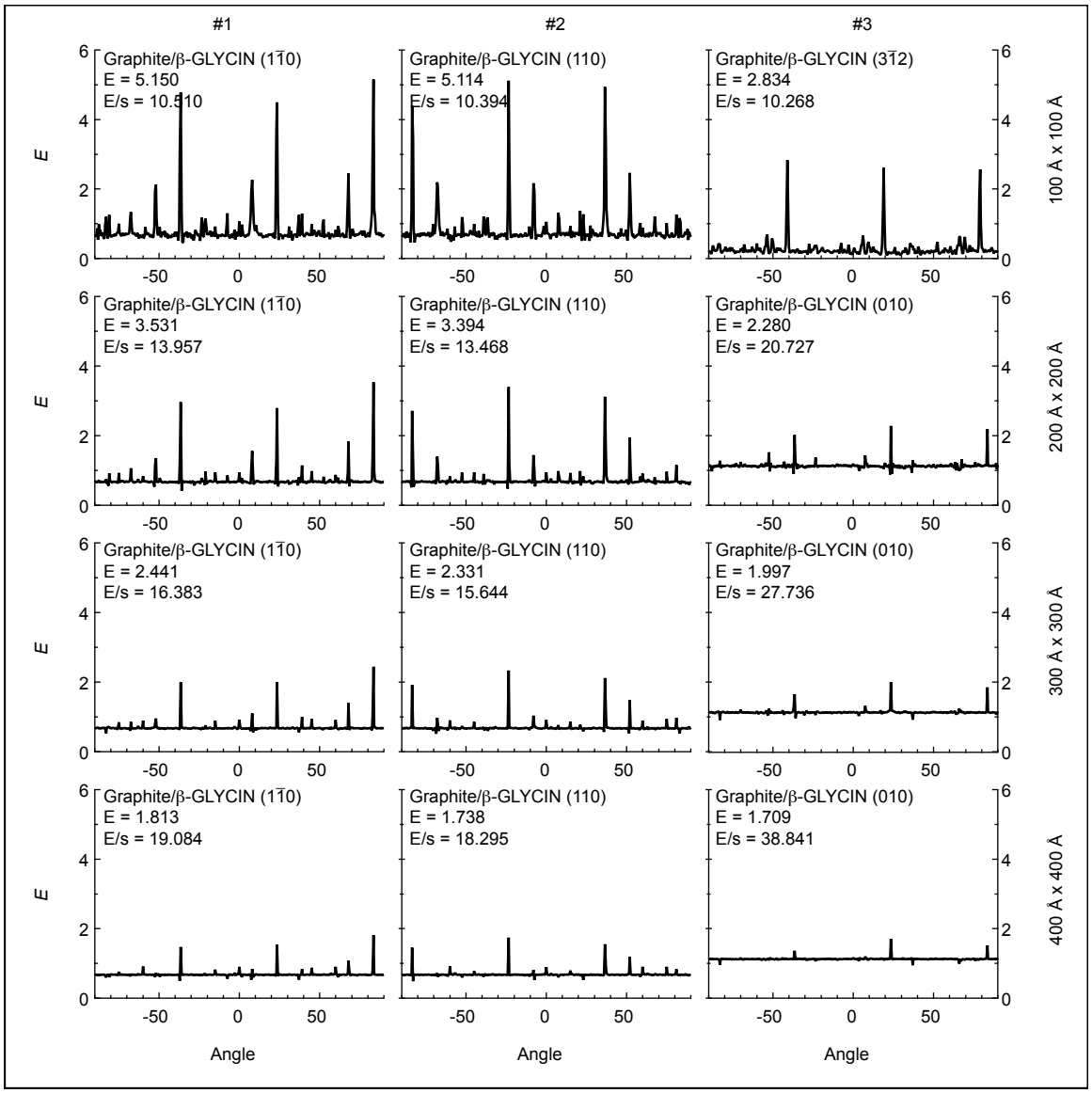

Figure S7. GRACE calculations for glycine and HOPG in terms of epitaxy score (*E*) versus azimuthal angle between the substrate lattice and the overlayer lattice. Columns are ordered from left to right with respect to the first, second, and third best epitaxy score. Rows are ordered from top to bottom with respect to area of calculation.

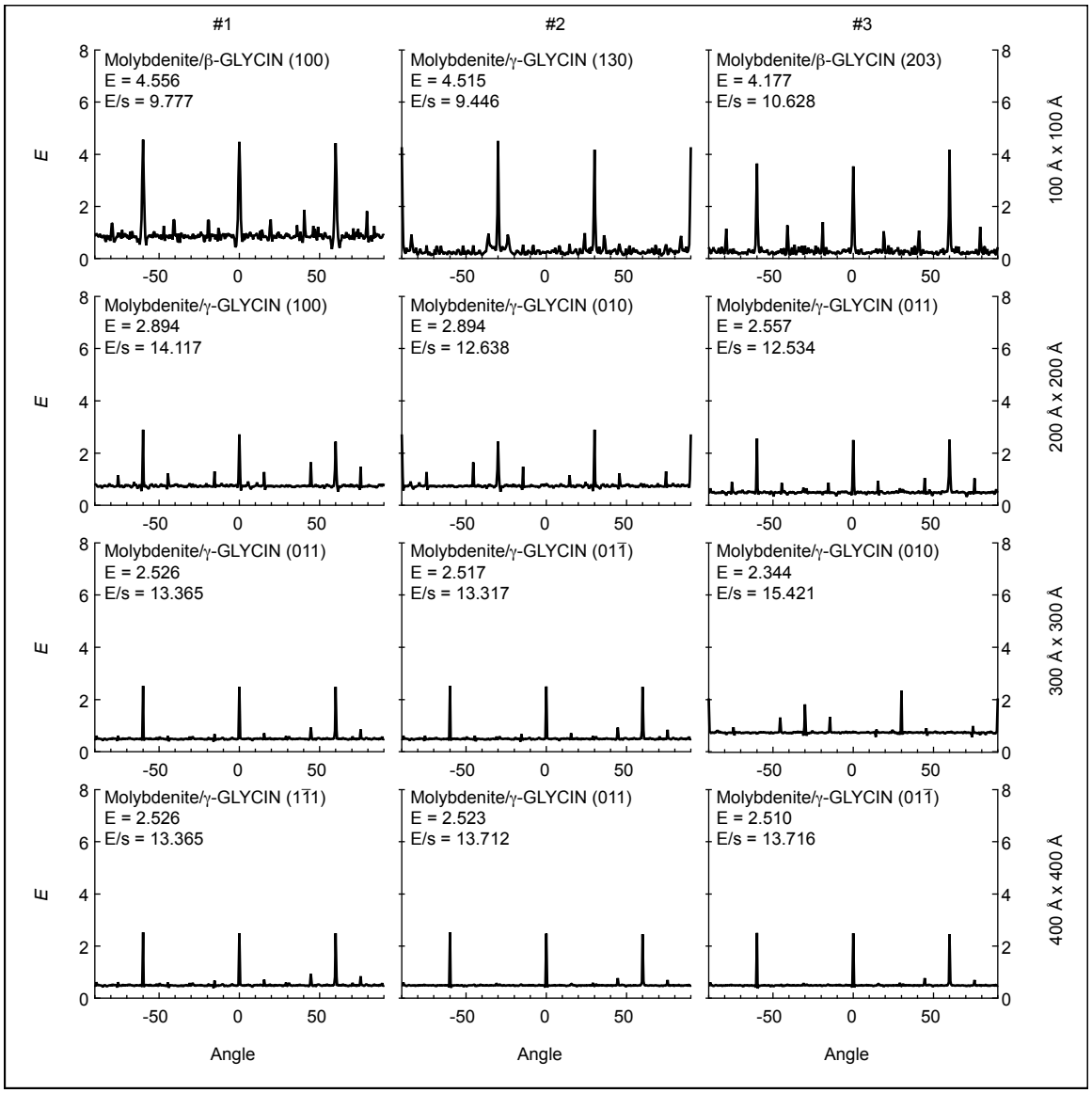

Figure S8. GRACE calculations for glycine and molybdenite in terms of epitaxy score (*E*) versus azimuthal angle between the substrate lattice and the overlayer lattice. Columns are ordered from left to right with respect to the first, second, and third best epitaxy score. Rows are ordered from top to bottom with respect to area of calculation.

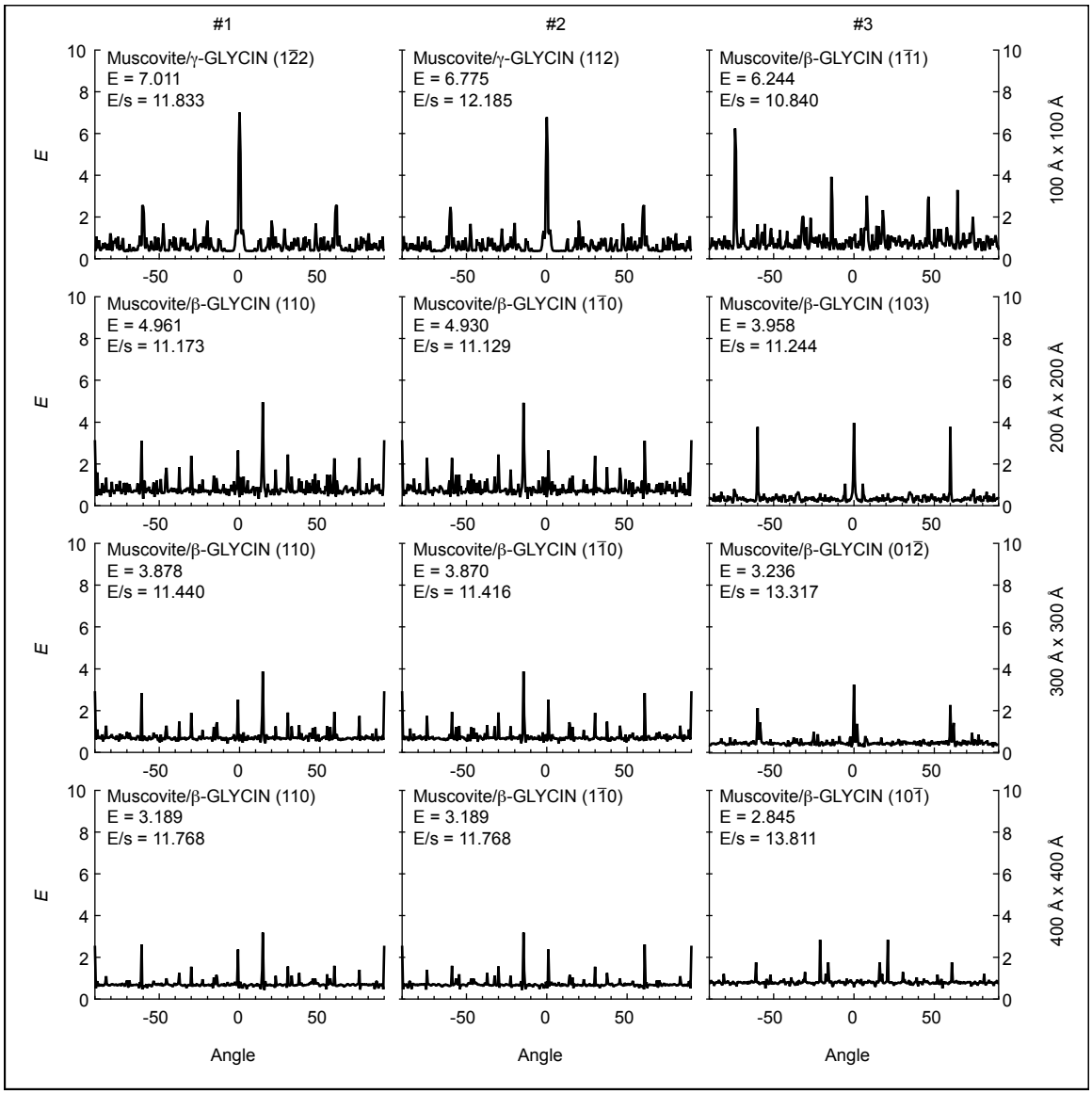

Figure S9. GRACE calculations for glycine and muscovite in terms of epitaxy score (*E*) versus azimuthal angle between the substrate lattice and the overlayer lattice. Columns are ordered from left to right with respect to the first, second, and third best epitaxy score. Rows are ordered from top to bottom with respect to area of calculation.

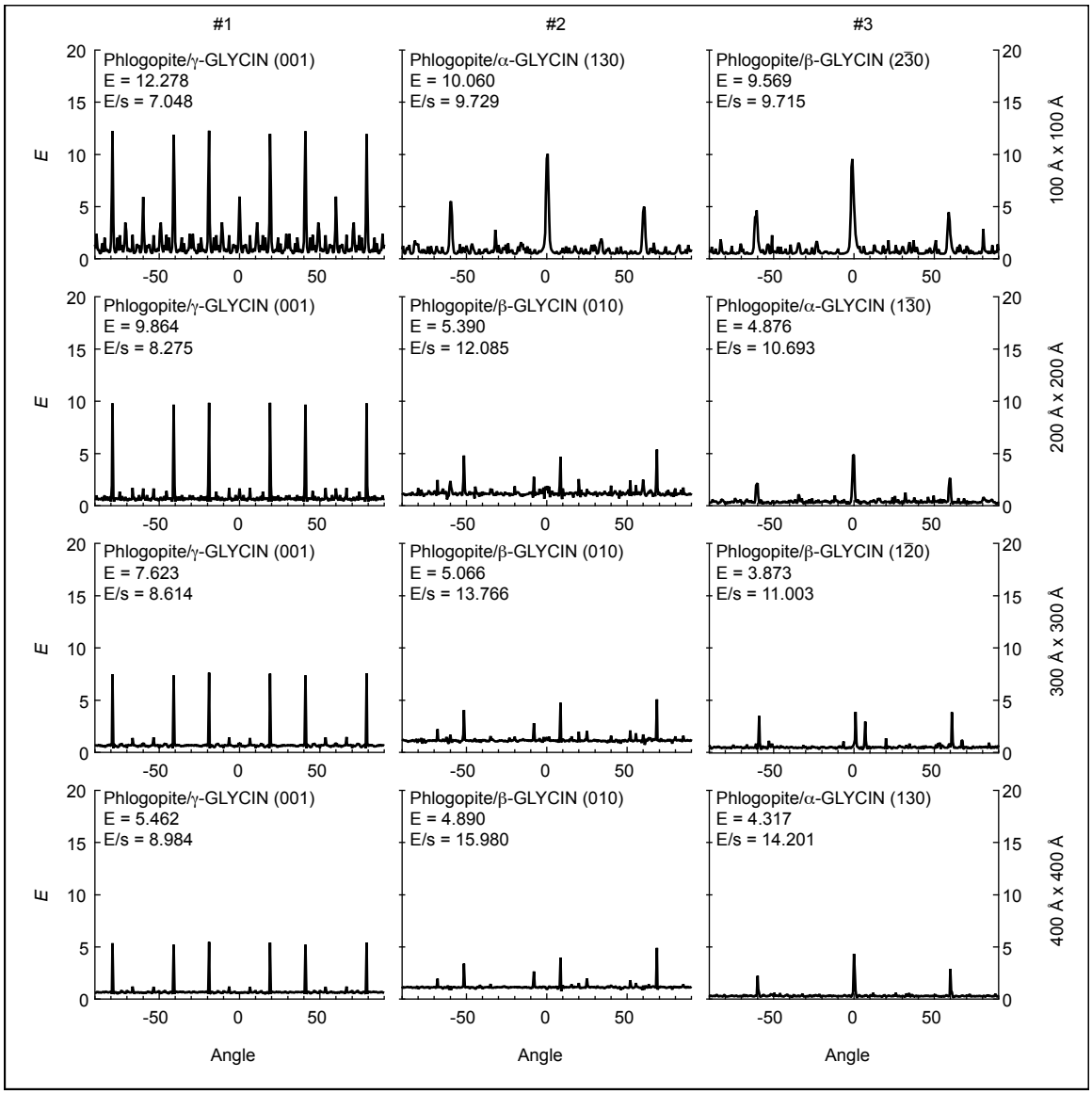

Figure S10. GRACE calculations for glycine and phlogopite in terms of epitaxy score (*E*) versus azimuthal angle between the substrate lattice and the overlayer lattice. Columns are ordered from left to right with respect to the first, second, and third best epitaxy score. Rows are ordered from top to bottom with respect to area of calculation.

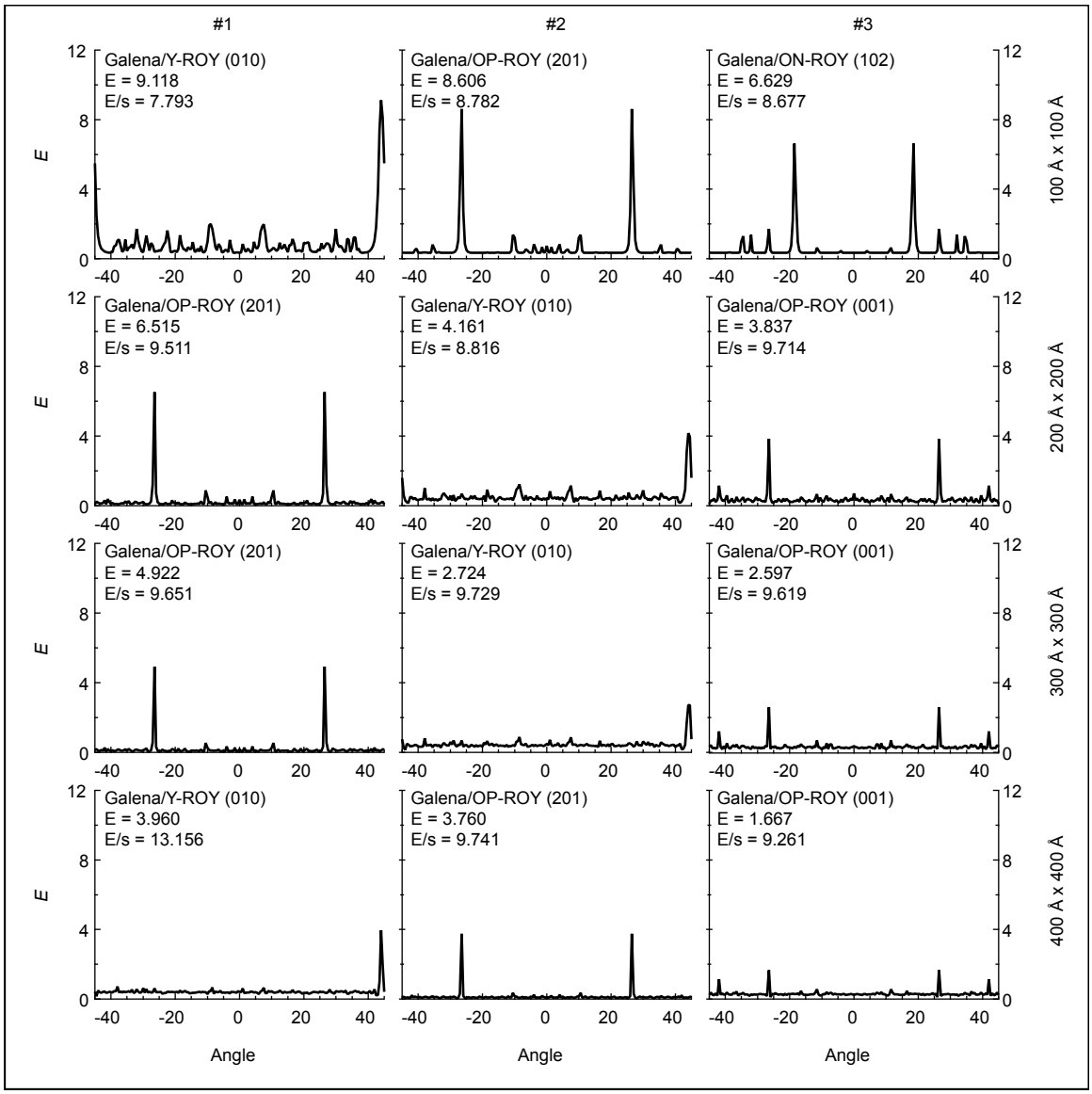

Figure S11. GRACE calculations for ROY and galena in terms of epitaxy score (*E*) versus azimuthal angle between the substrate lattice and the overlayer lattice. Columns are ordered from left to right with respect to the first, second, and third best epitaxy score. Rows are ordered from top to bottom with respect to area of calculation.

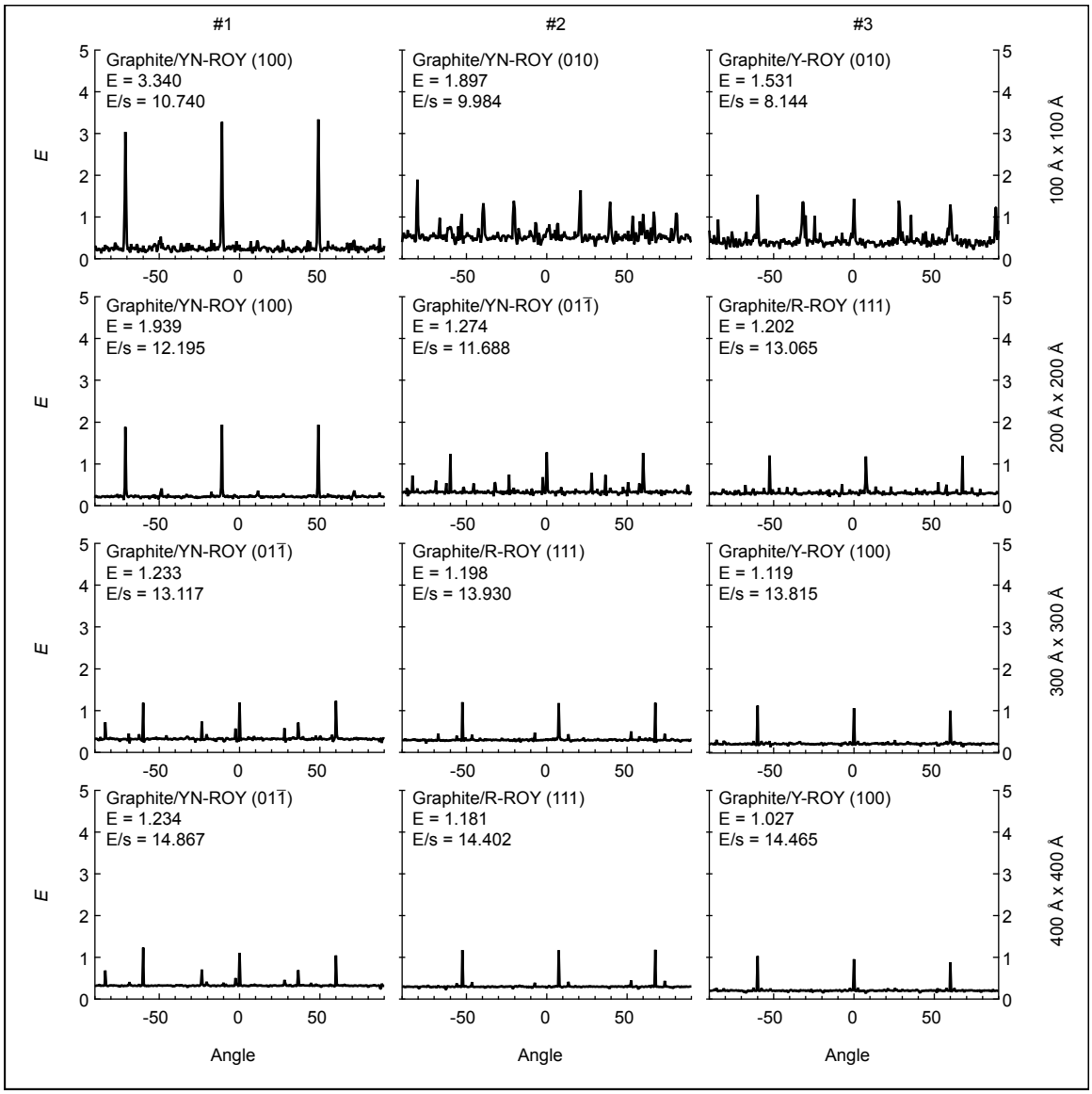

Figure S12. GRACE calculations for ROY and HOPG in terms of epitaxy score (*E*) versus azimuthal angle between the substrate lattice and the overlayer lattice. Columns are ordered from left to right with respect to the first, second, and third best epitaxy score. Rows are ordered from top to bottom with respect to area of calculation.

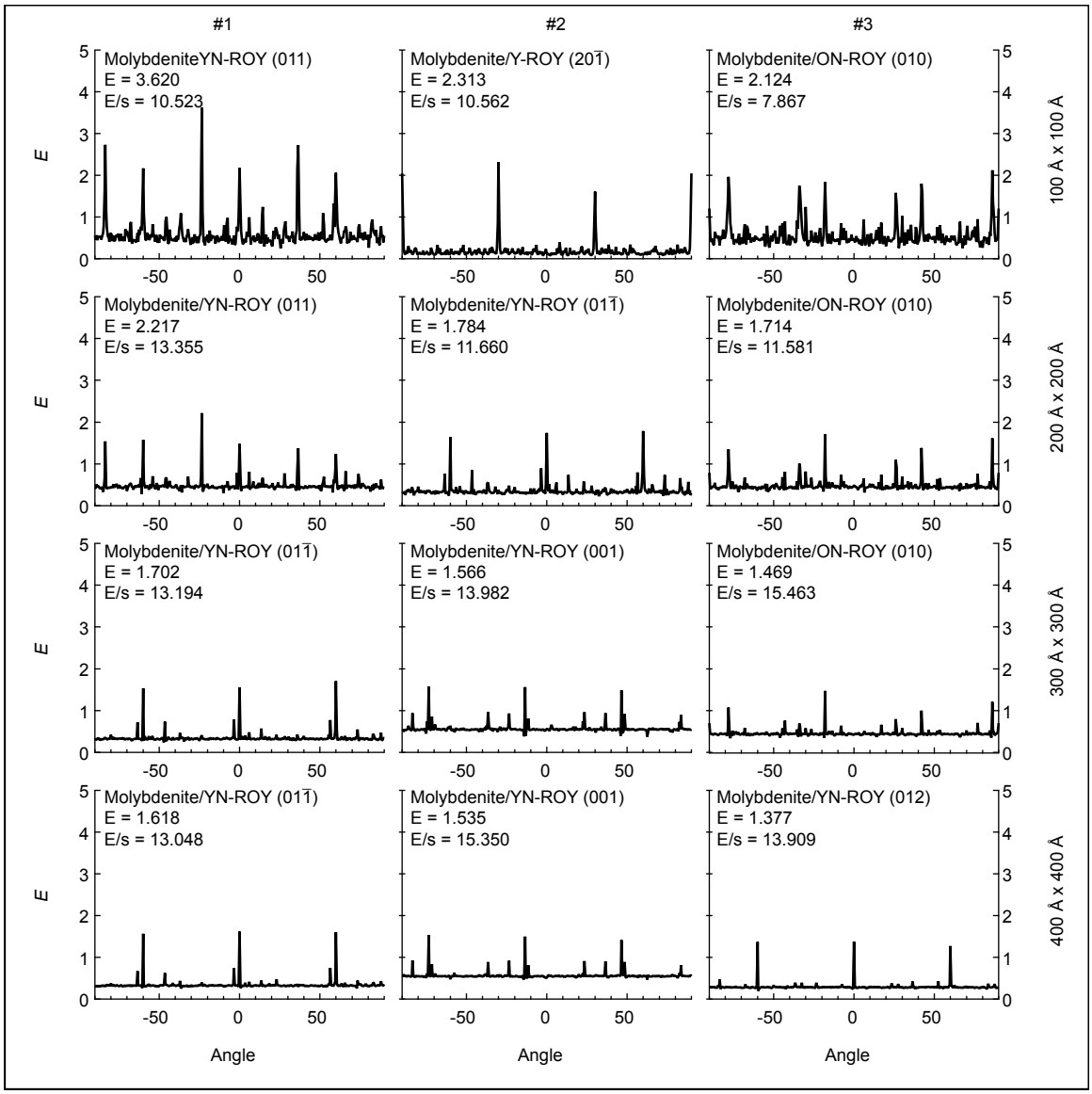

Figure S13. GRACE calculations for ROY and molybdenite in terms of epitaxy score (*E*) versus azimuthal angle between the substrate lattice and the overlayer lattice. Columns are ordered from left to right with respect to the first, second, and third best epitaxy score. Rows are ordered from top to bottom with respect to area of calculation.

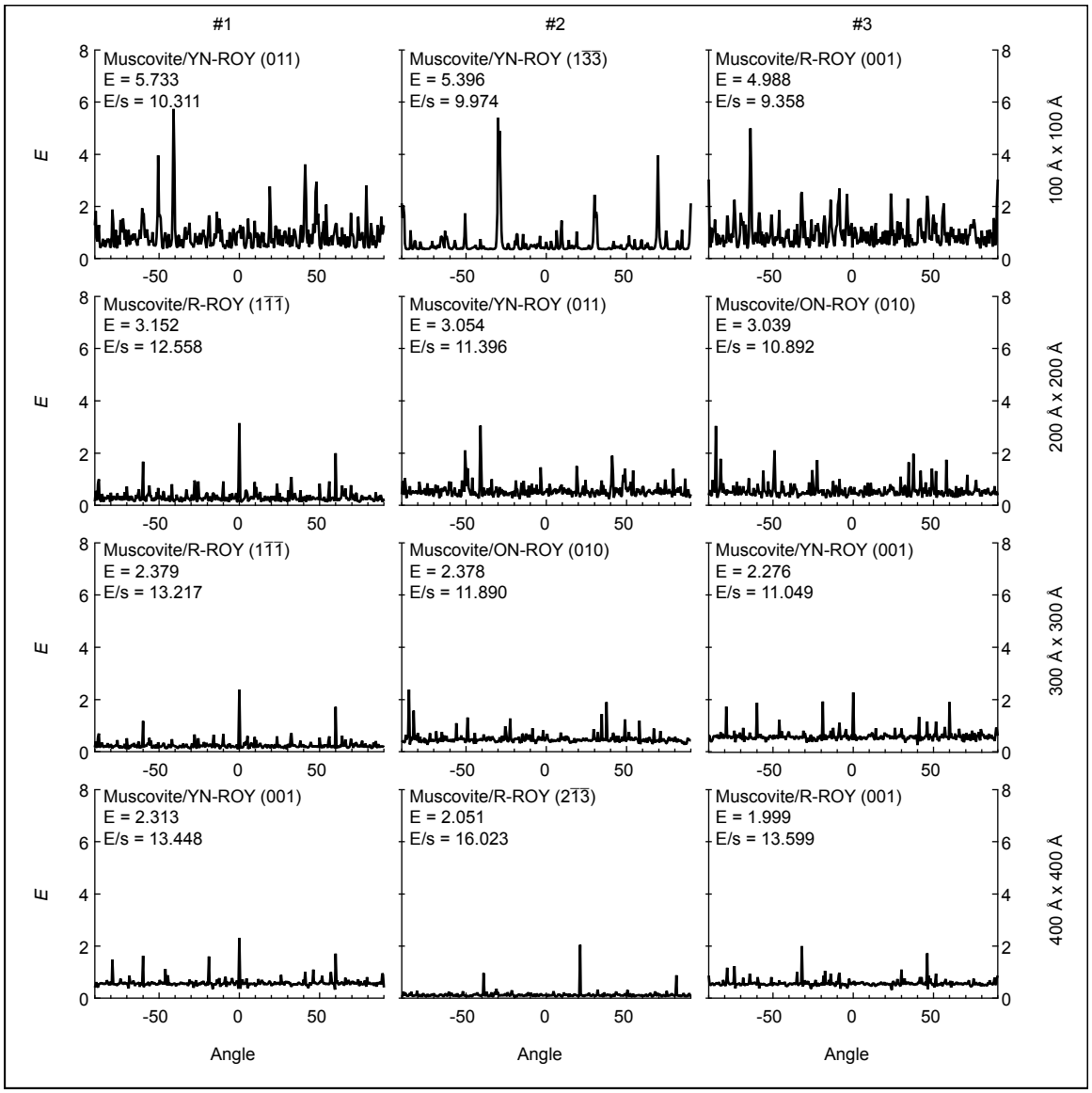

Figure S14. GRACE calculations for ROY and muscovite in terms of epitaxy score (*E*) versus azimuthal angle between the substrate lattice and the overlayer lattice. Columns are ordered from left to right with respect to the first, second, and third best epitaxy score. Rows are ordered from top to bottom with respect to area of calculation.

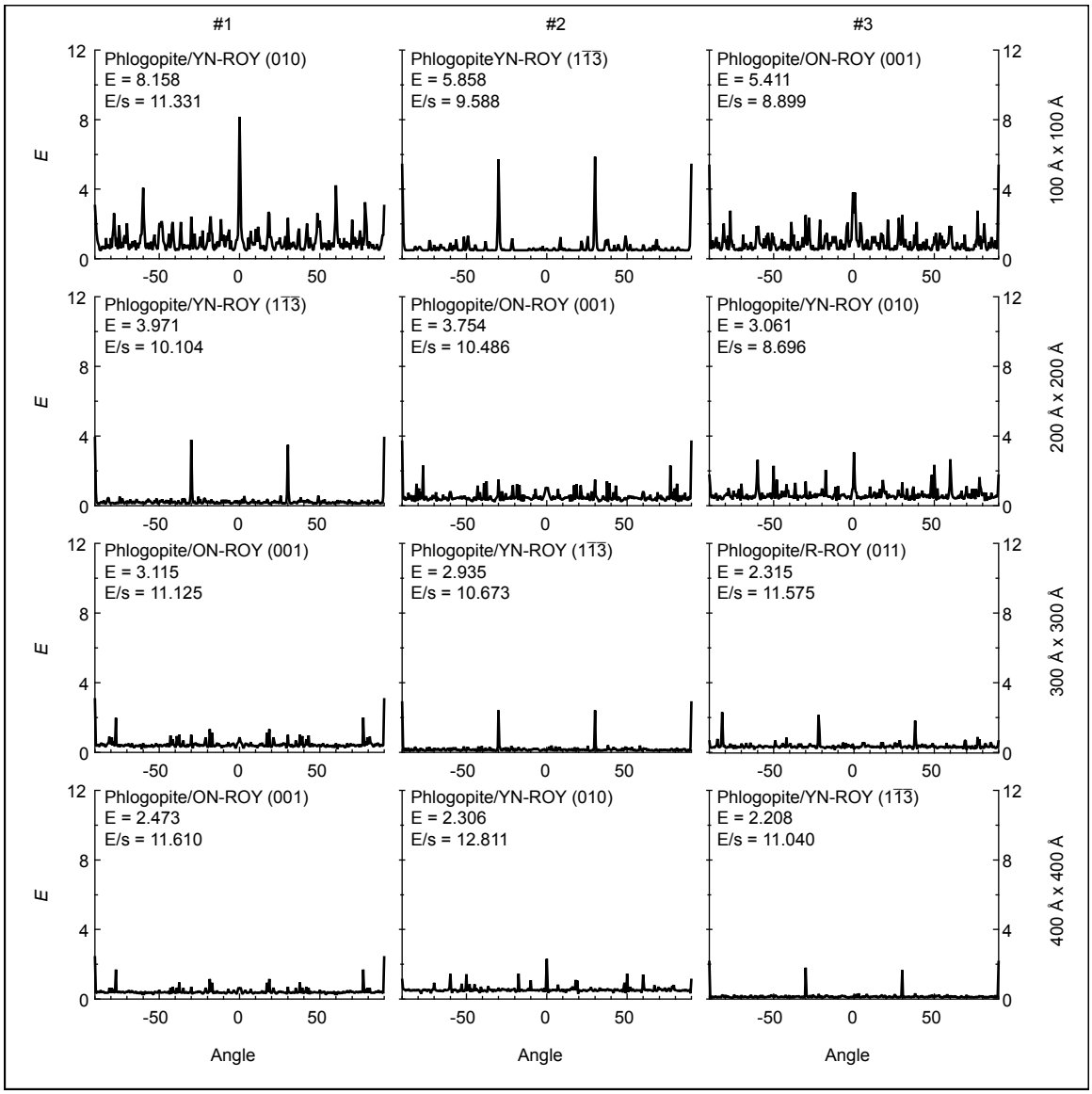

Figure S15. GRACE calculations for ROY and phlogopite in terms of epitaxy score (*E*) versus azimuthal angle between the substrate lattice and the overlayer lattice. Columns are ordered from left to right with respect to the first, second, and third best epitaxy score. Rows are ordered from top to bottom with respect to area of calculation.

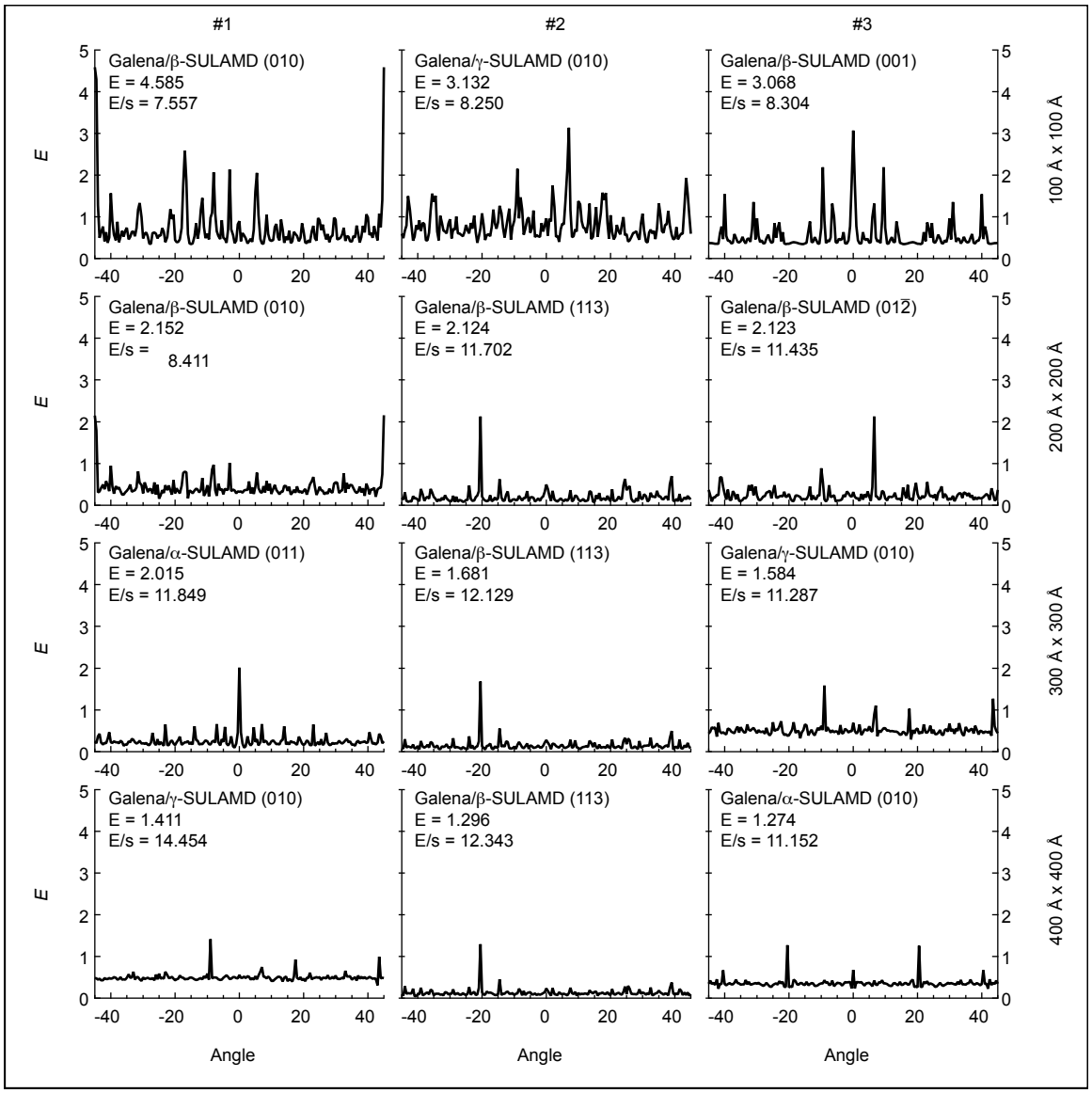

Figure S16. GRACE calculations for sulfanilamide and galena in terms of epitaxy score (*E*) versus azimuthal angle between the substrate lattice and the overlayer lattice. Columns are ordered from left to right with respect to the first, second, and third best epitaxy score. Rows are ordered from top to bottom with respect to area of calculation.

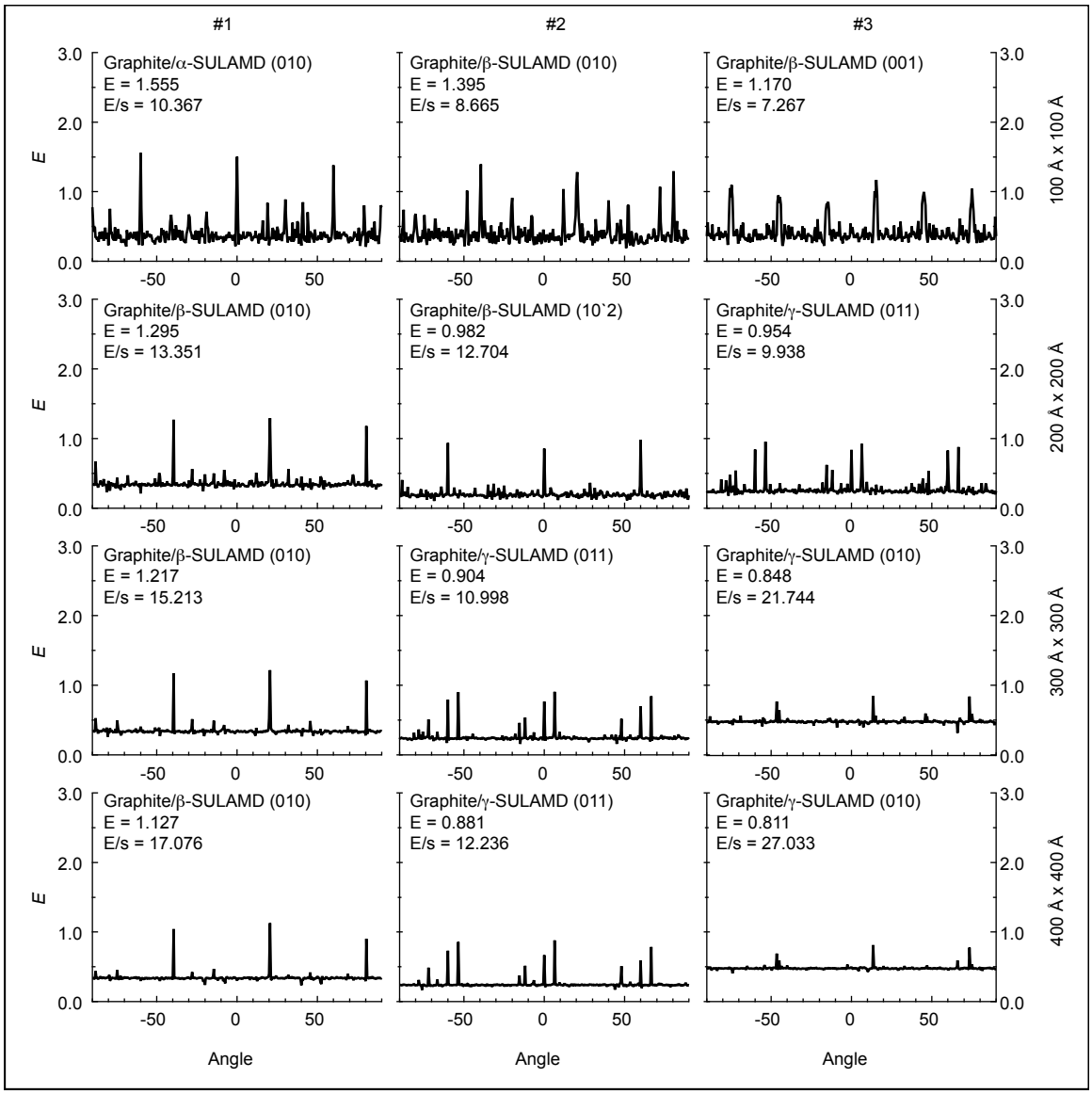

Figure S17. GRACE calculations for sulfanilamide and HOPG in terms of epitaxy score (*E*) versus azimuthal angle between the substrate lattice and the overlayer lattice. Columns are ordered from left to right with respect to the first, second, and third best epitaxy score. Rows are ordered from top to bottom with respect to area of calculation.

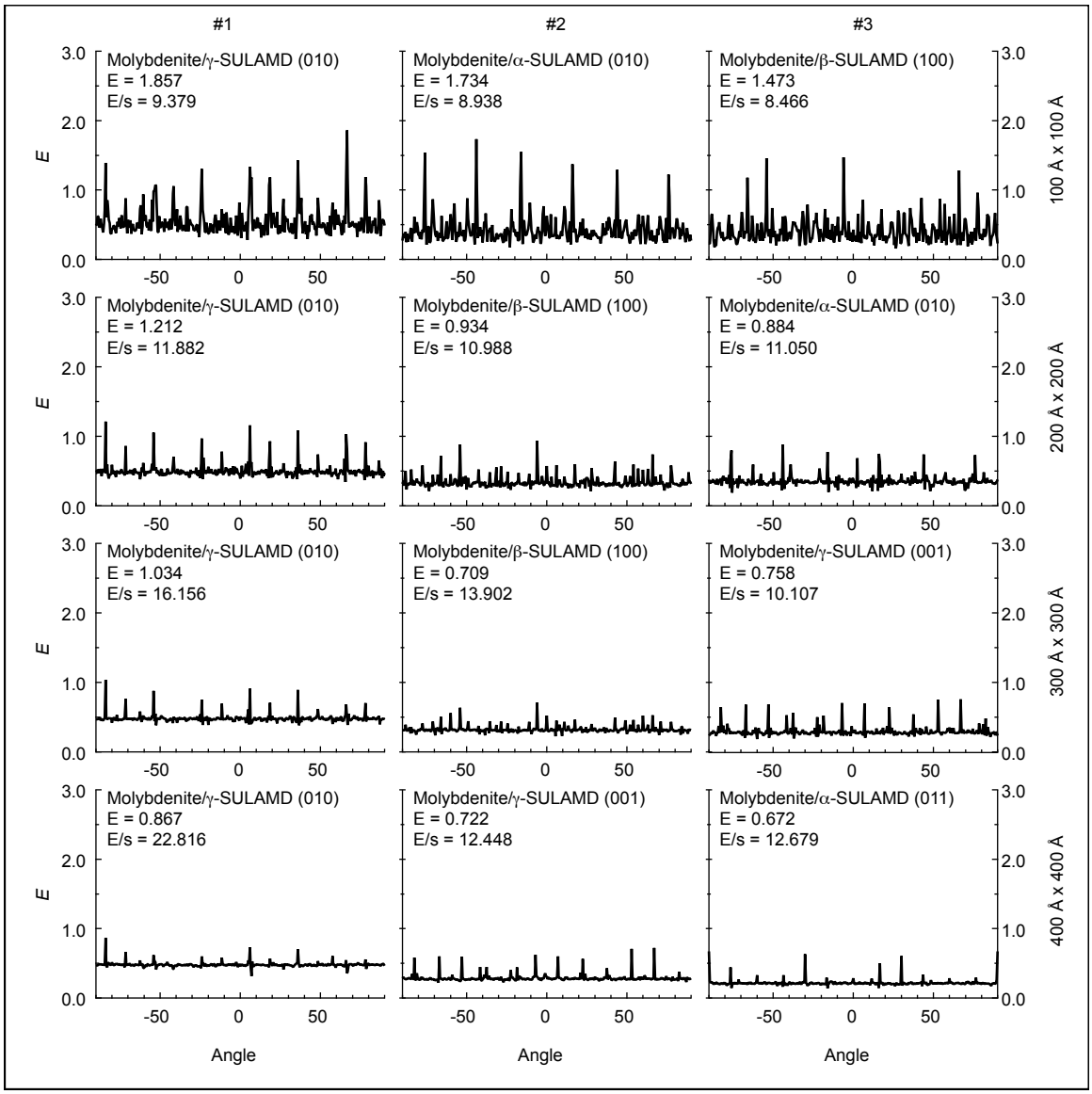

Figure S18. GRACE calculations for sulfanilamide and molybdenite in terms of epitaxy score (*E*) versus azimuthal angle between the substrate lattice and the overlayer lattice. Columns are ordered from left to right with respect to the first, second, and third best epitaxy score. Rows are ordered from top to bottom with respect to area of calculation.

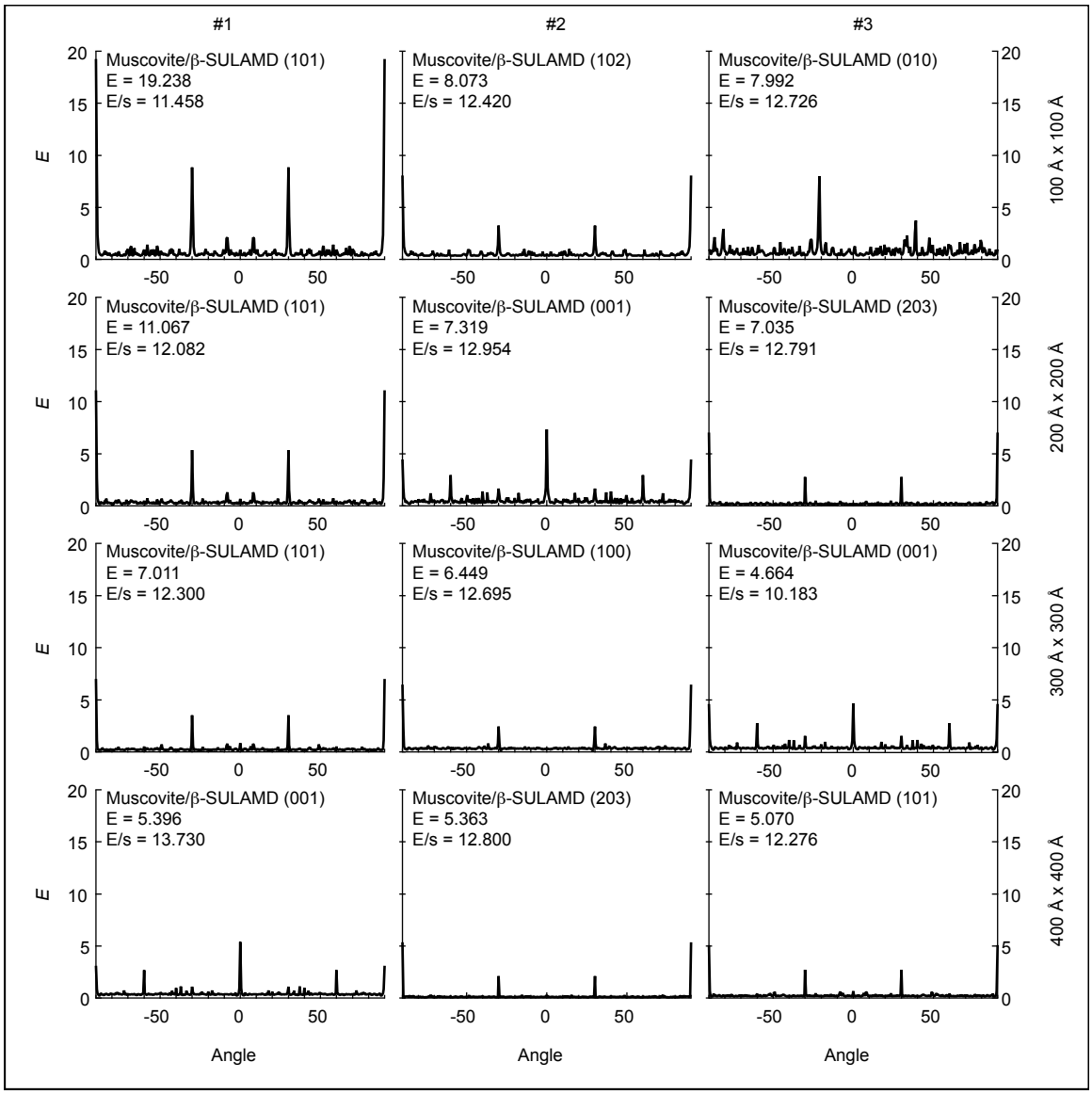

Figure S19. GRACE calculations for sulfanilamide and muscovite in terms of epitaxy score (*E*) versus azimuthal angle between the substrate lattice and the overlayer lattice. Columns are ordered from left to right with respect to the first, second, and third best epitaxy score. Rows are ordered from top to bottom with respect to area of calculation.

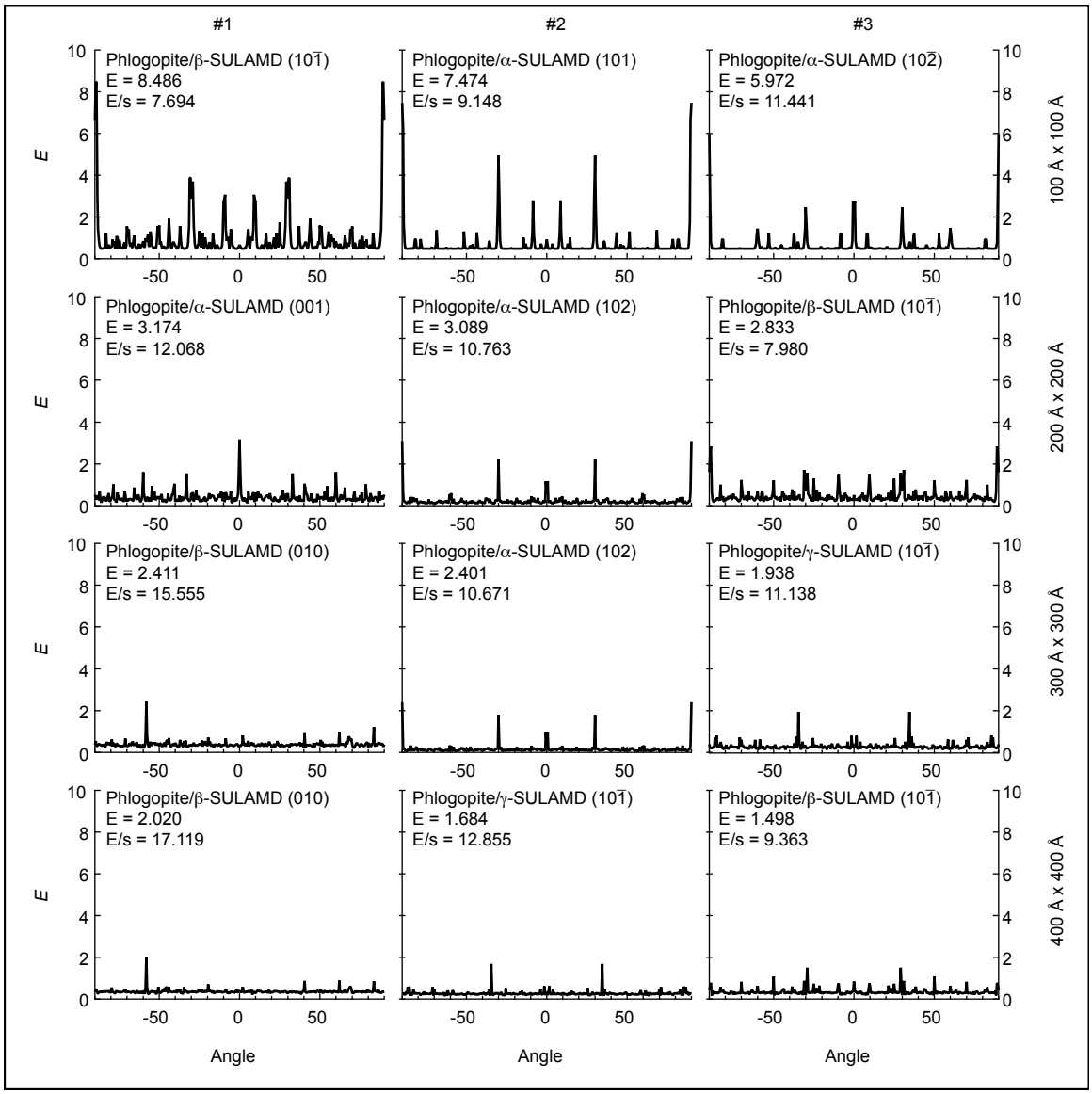

Figure S20. GRACE calculations for sulfanilamide and phlogopite in terms of epitaxy score (*E*) versus azimuthal angle between the substrate lattice and the overlayer lattice. Columns are ordered from left to right with respect to the first, second, and third best epitaxy score. Rows are ordered from top to bottom with respect to area of calculation.

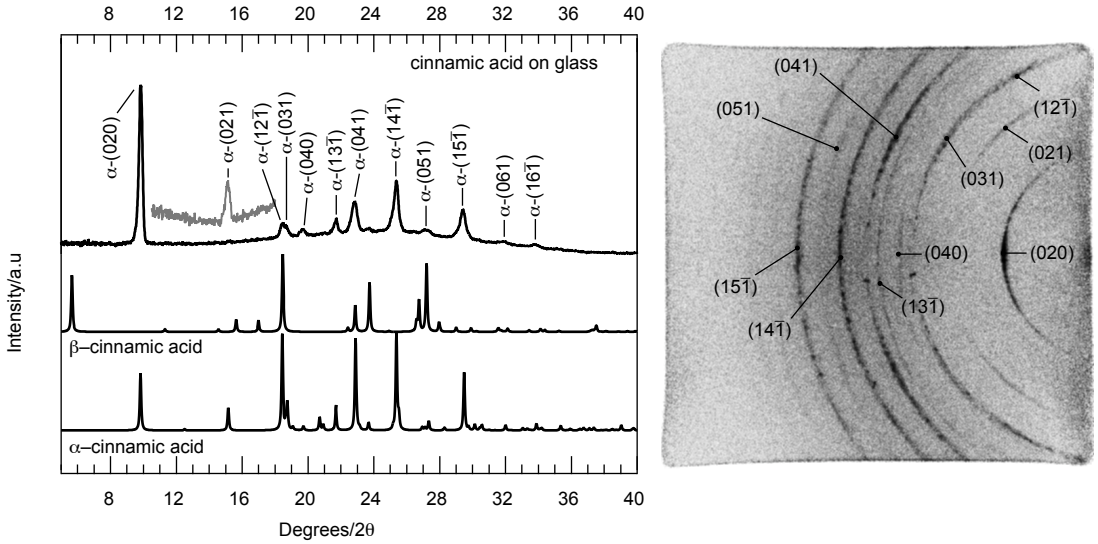

Figure S21. X-ray Microdiffraction data for *trans*-cinnamic acid on glass. Lower traces are simulated powder patterns calculated from the single crystal structures for relevant polymorphs. Gray traces indicate data acquired by secondary integration of portions of the full two-dimensional frame. Secondary integrations were necessary to avoid the regions of strong signal from the crystalline substrates.

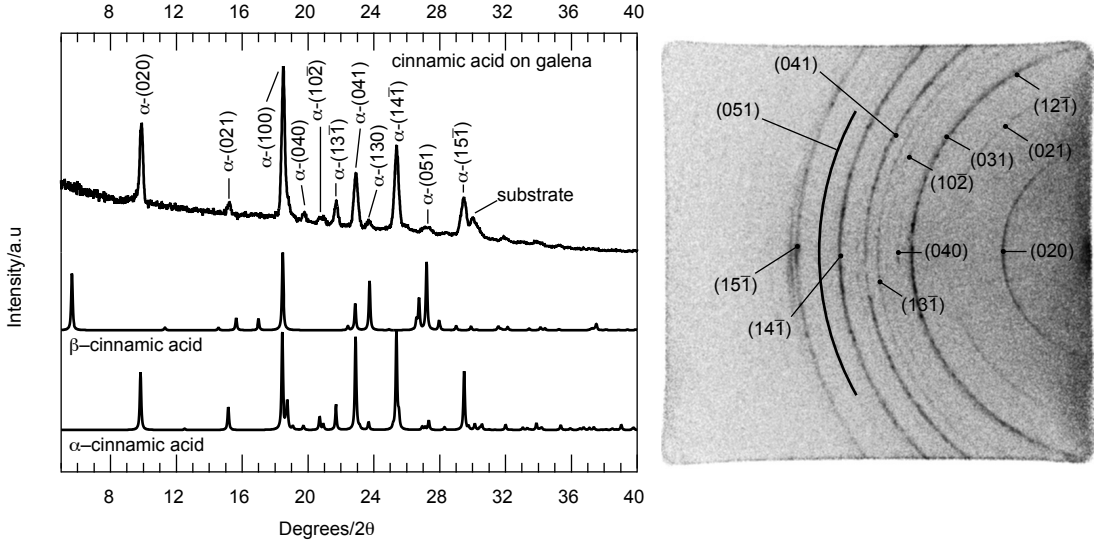

Figure S22. X-ray Microdiffraction data for *trans*-cinnamic acid on galena. Lower traces are simulated powder patterns calculated from the single crystal structures for relevant polymorphs. Gray traces indicate data acquired by secondary integration of portions of the full two-dimensional frame. Secondary integrations were necessary to avoid the regions of strong signal from the crystalline substrates.

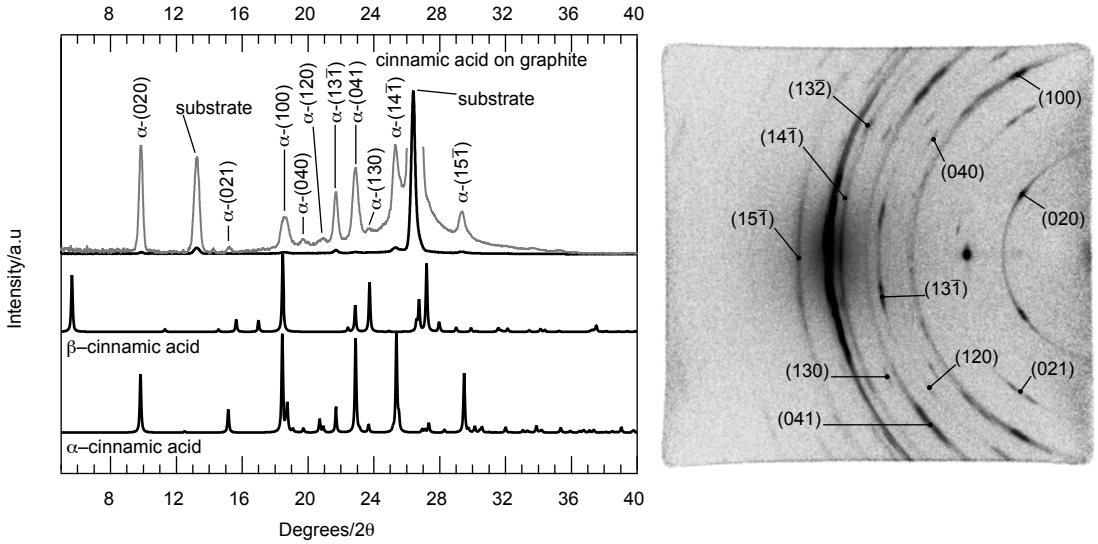

Figure S23. X-ray Microdiffraction data for *trans*-cinnamic acid on HOPG. Lower traces are simulated powder patterns calculated from the single crystal structures for relevant polymorphs. Gray traces indicate data acquired by secondary integration of portions of the full two-dimensional frame. Secondary integrations were necessary to avoid the regions of strong signal from the crystalline substrates.

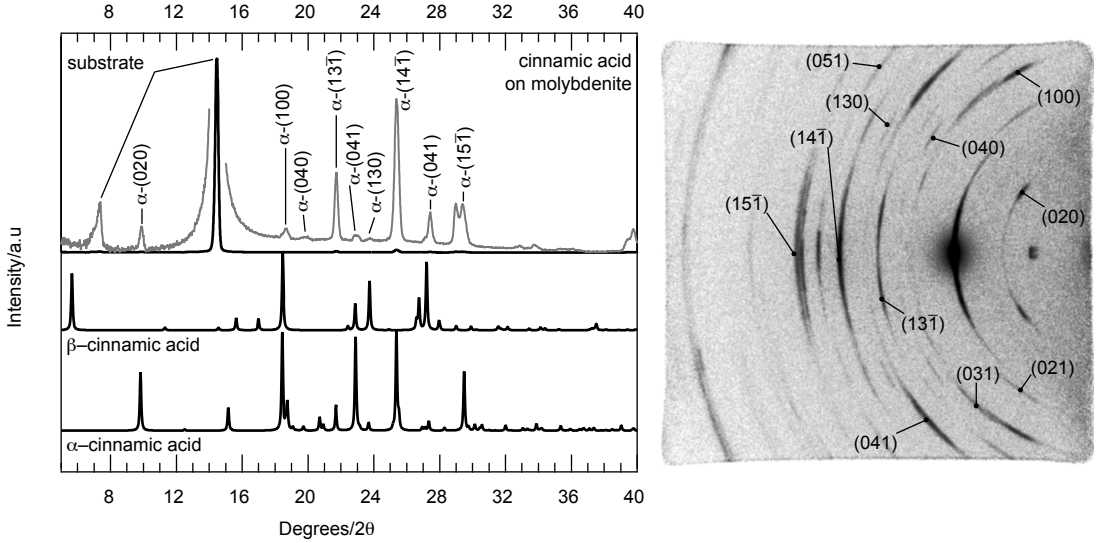

Figure S24. X-ray Microdiffraction data for *trans*-cinnamic acid on molybdenite. Lower traces are simulated powder patterns calculated from the single crystal structures for relevant polymorphs. Gray traces indicate data acquired by secondary integration of portions of the full two-dimensional frame. Secondary integrations were necessary to avoid the regions of strong signal from the crystalline substrates.

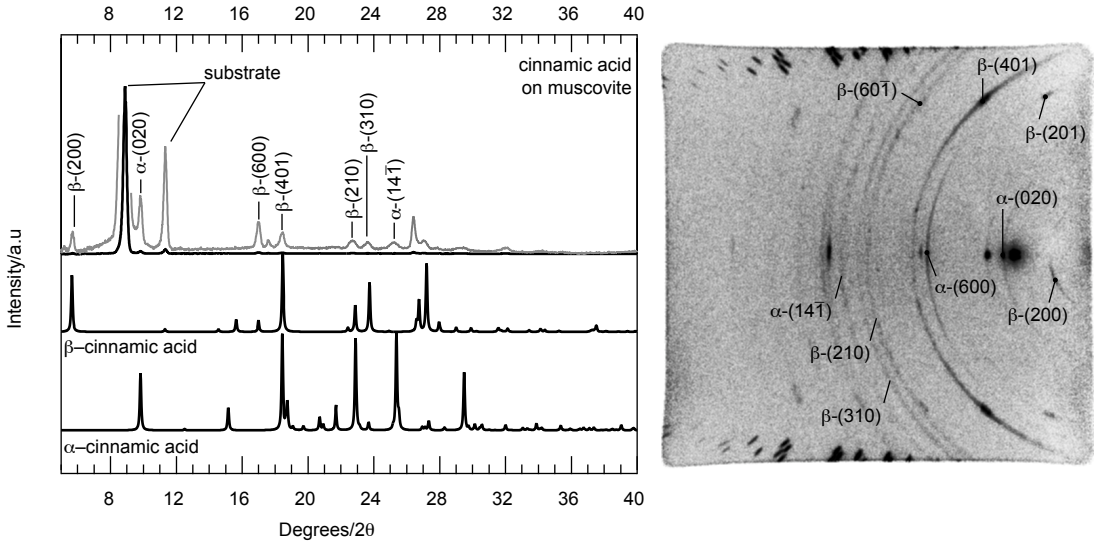

Figure S25. X-ray Microdiffraction data for *trans*-cinnamic acid on muscovite. Lower traces are simulated powder patterns calculated from the single crystal structures for relevant polymorphs. Gray traces indicate data acquired by secondary integration of portions of the full two-dimensional frame. Secondary integrations were necessary to avoid the regions of strong signal from the crystalline substrates.

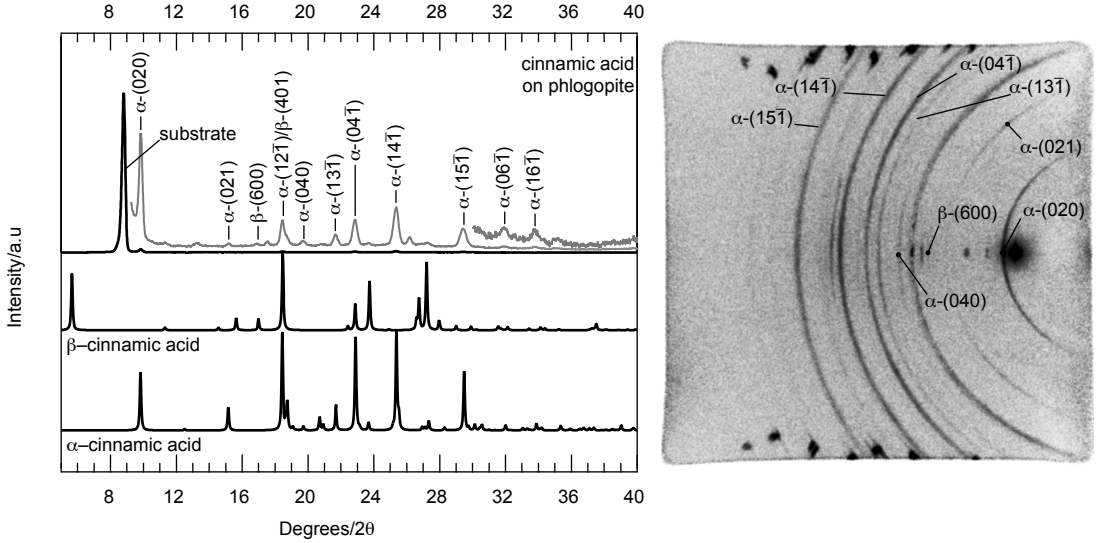

Figure S26. X-ray Microdiffraction data for *trans*-cinnamic acid on phlogopite. Lower traces are simulated powder patterns calculated from the single crystal structures for relevant polymorphs. Gray traces indicate data acquired by secondary integration of portions of the full two-dimensional frame. Secondary integrations were necessary to avoid the regions of strong signal from the crystalline substrates.

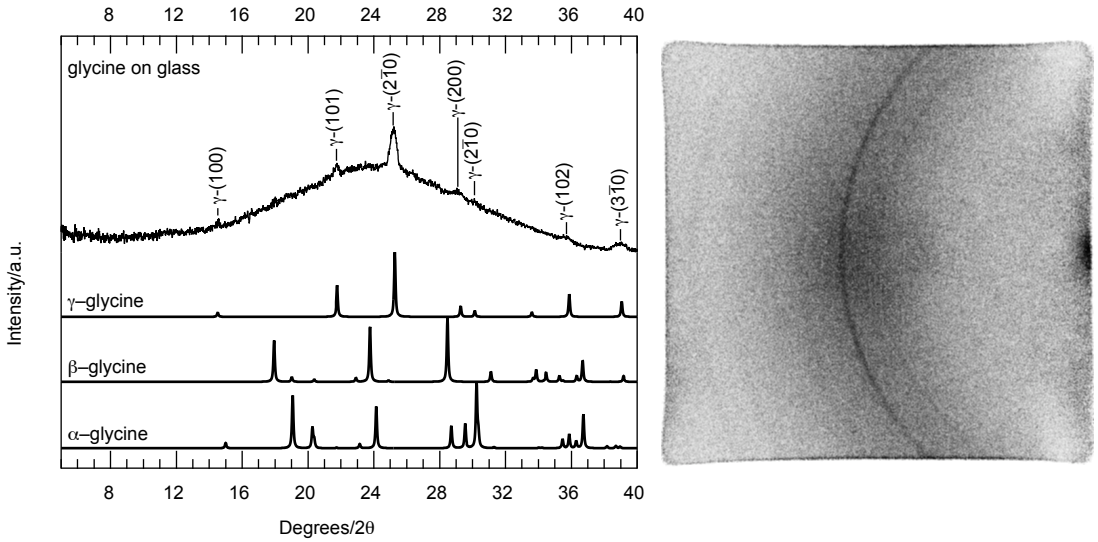

Figure S27. X-ray Microdiffraction data for glycine on glass. Lower traces are simulated powder patterns calculated from the single crystal structures for relevant polymorphs. Gray traces indicate data acquired by secondary integration of portions of the full two-dimensional frame. Secondary integrations were necessary to avoid the regions of strong signal from the crystalline substrates.

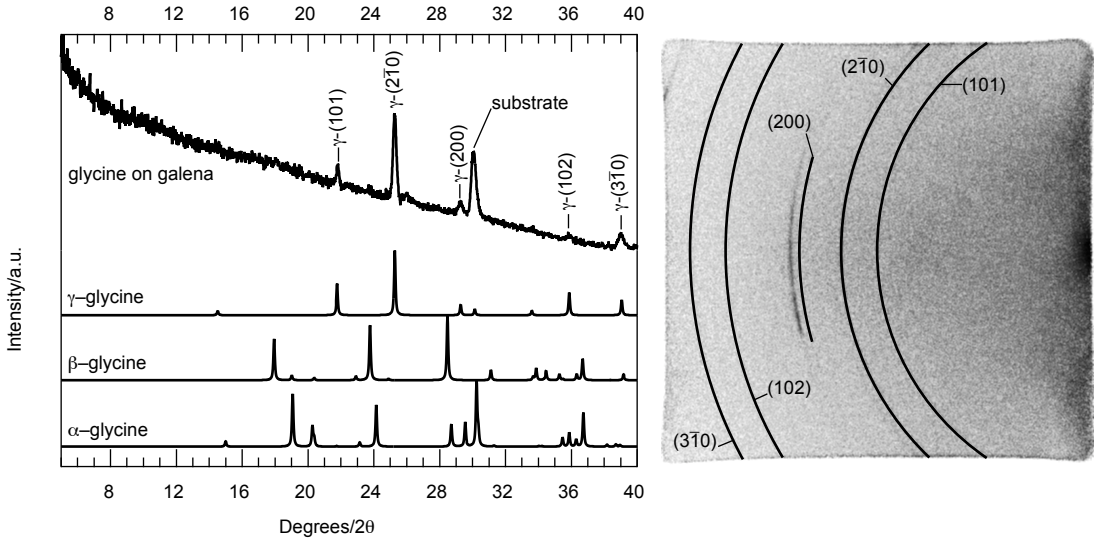

Figure S28. X-ray Microdiffraction data for glycine on galena. Lower traces are simulated powder patterns calculated from the single crystal structures for relevant polymorphs. Gray traces indicate data acquired by secondary integration of portions of the full two-dimensional frame. Secondary integrations were necessary to avoid the regions of strong signal from the crystalline substrates.

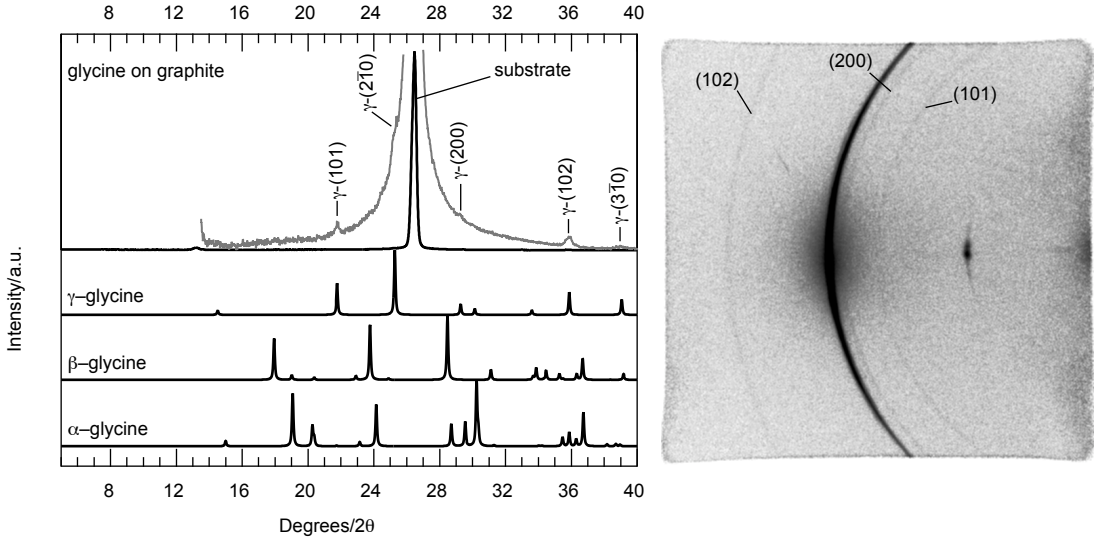

Figure S29. X-ray Microdiffraction data for glycine on HOPG. Lower traces are simulated powder patterns calculated from the single crystal structures for relevant polymorphs. Gray traces indicate data acquired by secondary integration of portions of the full two-dimensional frame. Secondary integrations were necessary to avoid the regions of strong signal from the crystalline substrates.

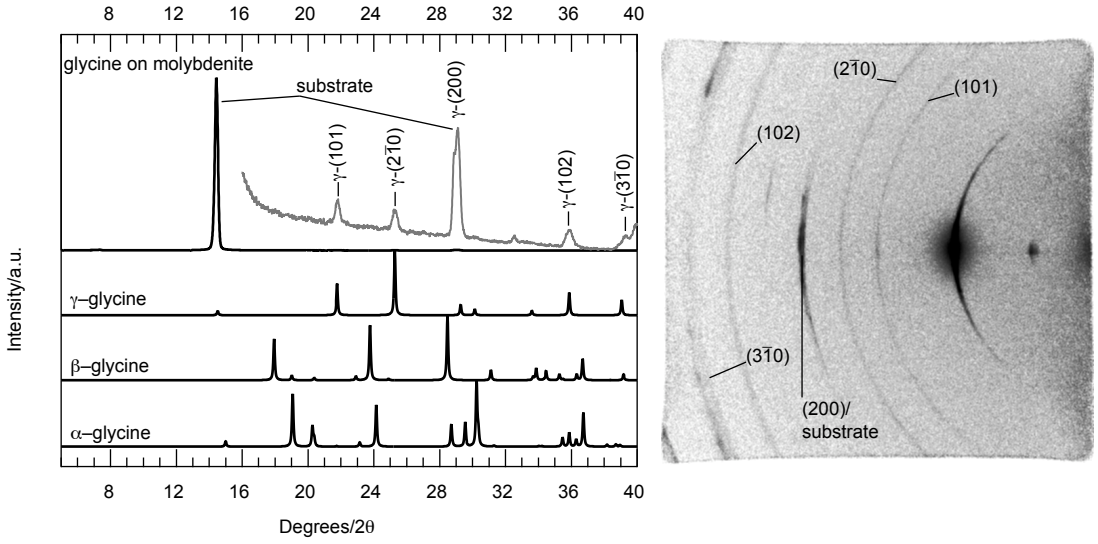

Figure S30. X-ray Microdiffraction data for glycine on molybdenite. Lower traces are simulated powder patterns calculated from the single crystal structures for relevant polymorphs. Gray traces indicate data acquired by secondary integration of portions of the full two-dimensional frame. Secondary integrations were necessary to avoid the regions of strong signal from the crystalline substrates.

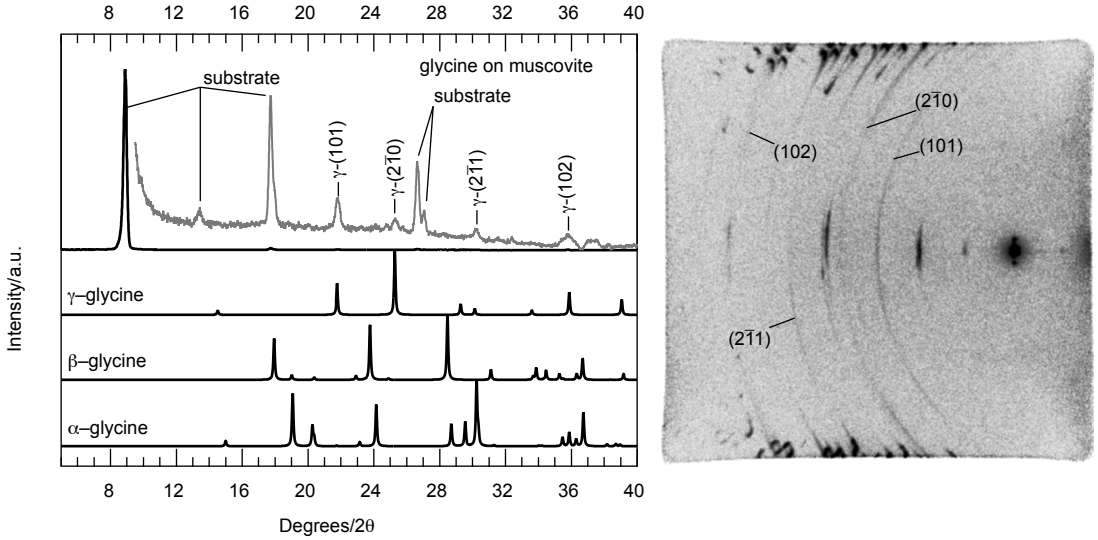

Figure S31. X-ray Microdiffraction data for glycine on muscovite. Lower traces are simulated powder patterns calculated from the single crystal structures for relevant polymorphs. Gray traces indicate data acquired by secondary integration of portions of the full two-dimensional frame. Secondary integrations were necessary to avoid the regions of strong signal from the crystalline substrates.

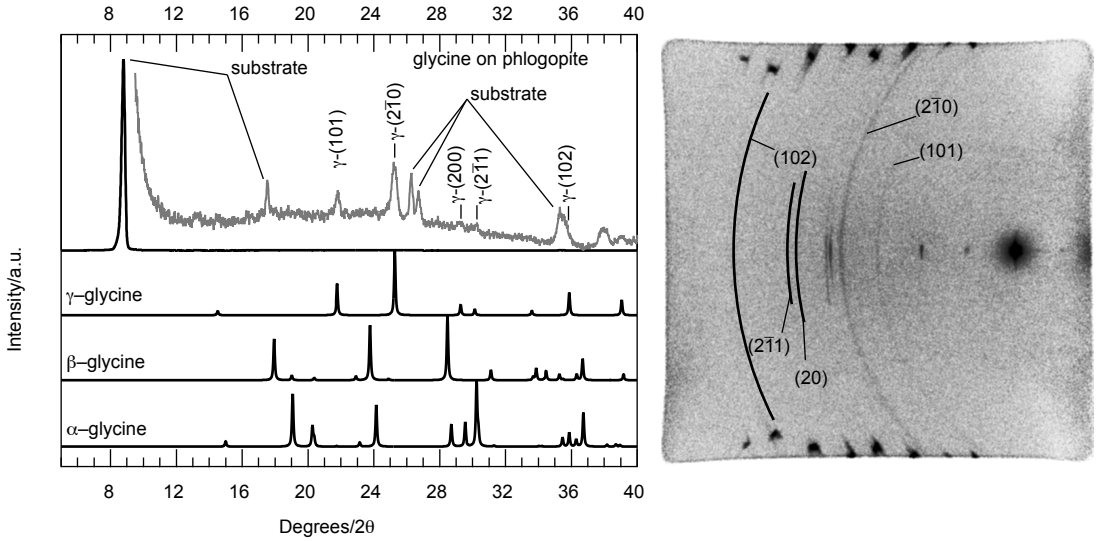

Figure S32. X-ray Microdiffraction data for glycine on phlogopite. Lower traces are simulated powder patterns calculated from the single crystal structures for relevant polymorphs. Gray traces indicate data acquired by secondary integration of portions of the full two-dimensional frame. Secondary integrations were necessary to avoid the regions of strong signal from the crystalline substrates.

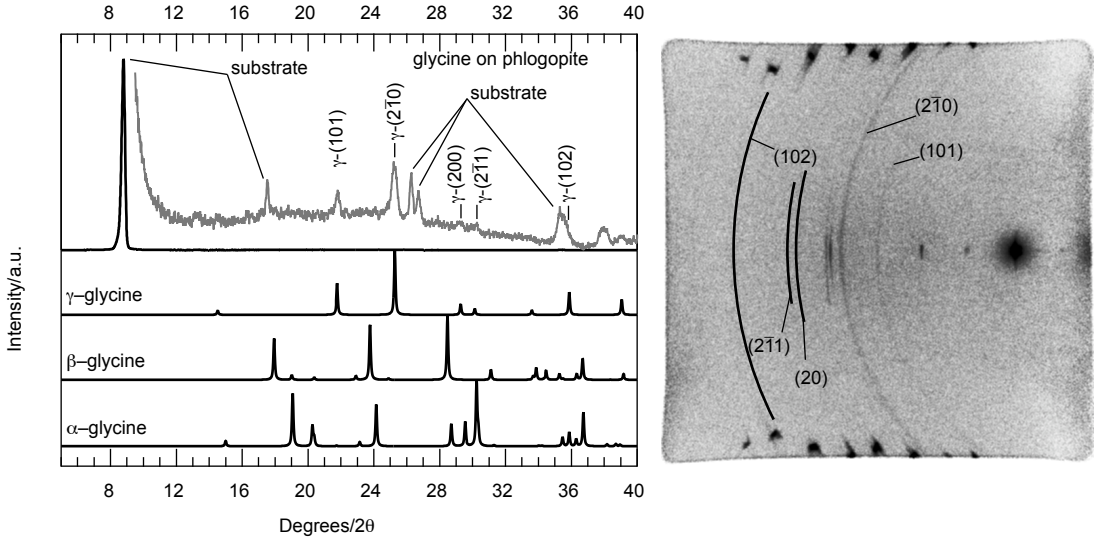

Figure S33. X-ray Microdiffraction data for ROY on glass. Lower traces are simulated powder patterns calculated from the single crystal structures for relevant polymorphs. Gray traces indicate data acquired by secondary integration of portions of the full two-dimensional frame. Secondary integrations were necessary to avoid the regions of strong signal from the crystalline substrates.

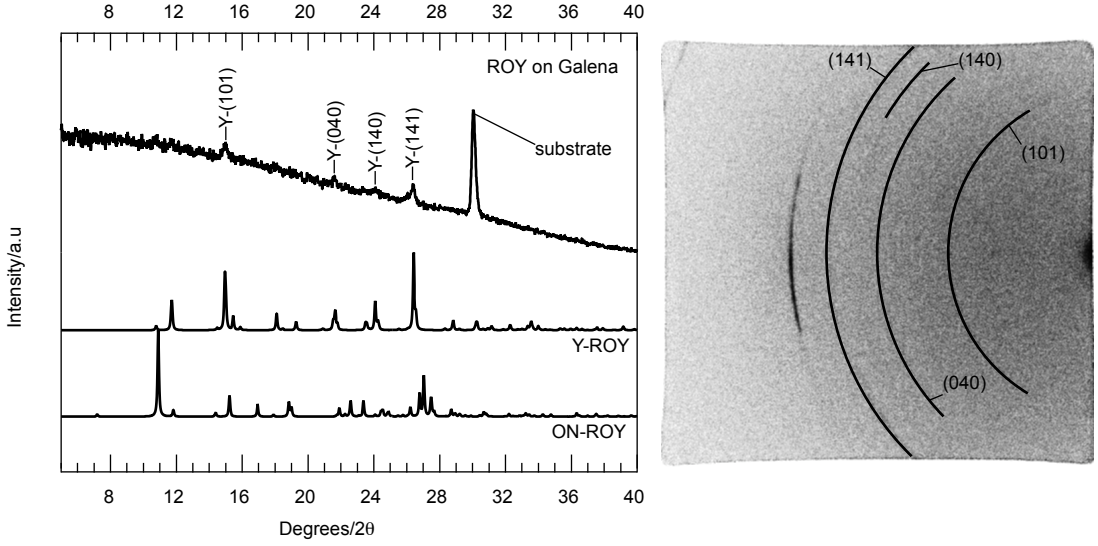

Figure S34. X-ray Microdiffraction data for ROY on galena. Lower traces are simulated powder patterns calculated from the single crystal structures for relevant polymorphs. Gray traces indicate data acquired by secondary integration of portions of the full two-dimensional frame. Secondary integrations were necessary to avoid the regions of strong signal from the crystalline substrates.

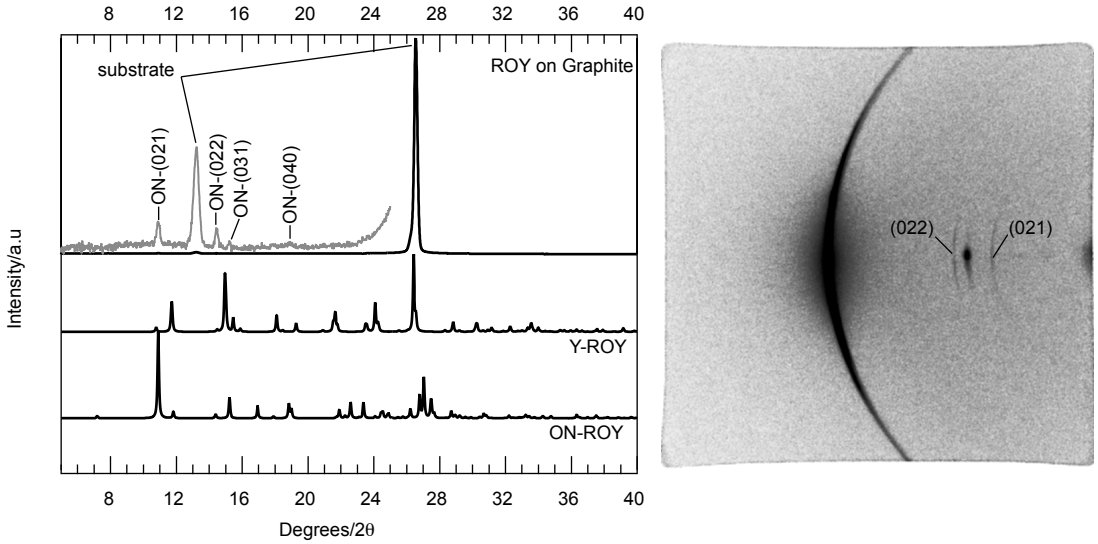

Figure S35. X-ray Microdiffraction data for ROY on HOPG. Lower traces are simulated powder patterns calculated from the single crystal structures for relevant polymorphs. Gray traces indicate data acquired by secondary integration of portions of the full two-dimensional frame. Secondary integrations were necessary to avoid the regions of strong signal from the crystalline substrates.

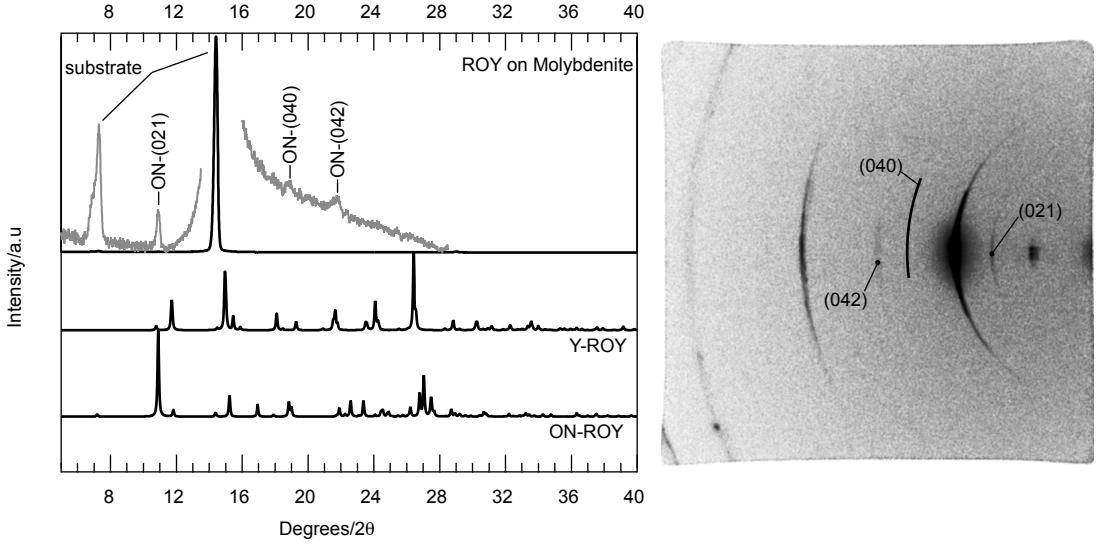

Figure S36. X-ray Microdiffraction data for ROY on molybdenite. Lower traces are simulated powder patterns calculated from the single crystal structures for relevant polymorphs. Gray traces indicate data acquired by secondary integration of portions of the full two-dimensional frame. Secondary integrations were necessary to avoid the regions of strong signal from the crystalline substrates.

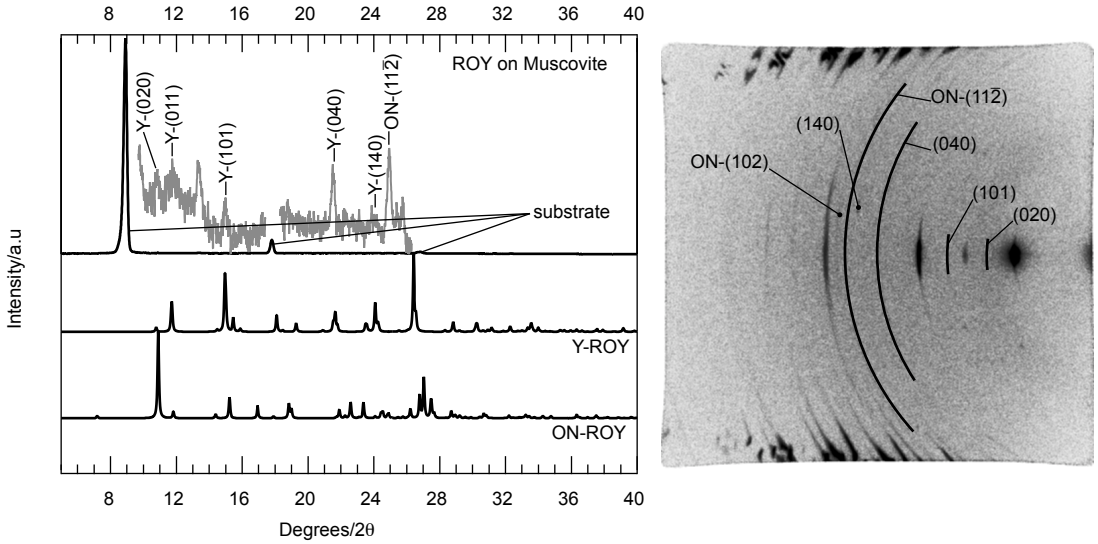

Figure S37. X-ray Microdiffraction data for ROY on muscovite. Lower traces are simulated powder patterns calculated from the single crystal structures for relevant polymorphs. Gray traces indicate data acquired by secondary integration of portions of the full two-dimensional frame. Secondary integrations were necessary to avoid the regions of strong signal from the crystalline substrates.

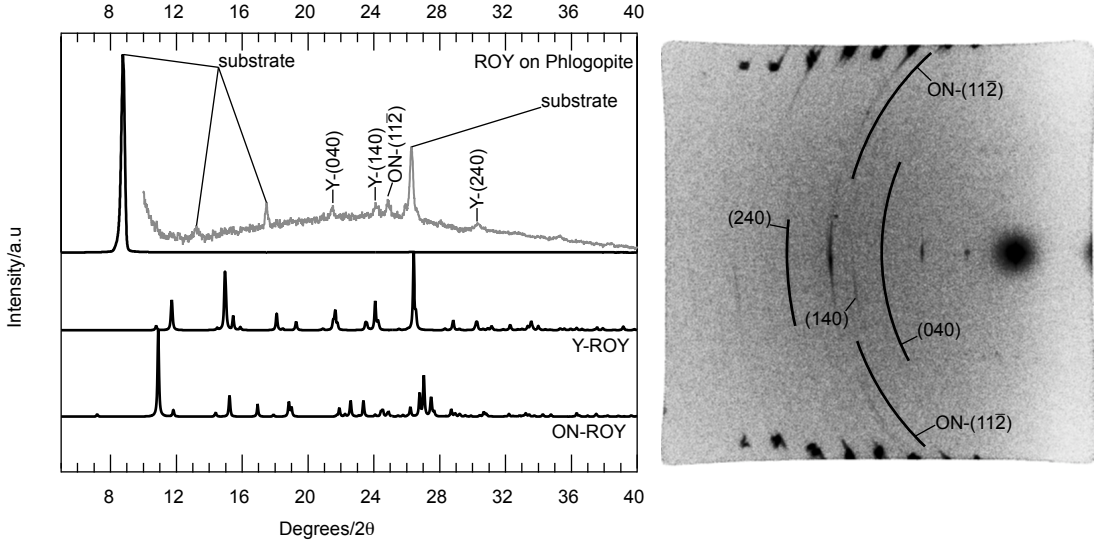

Figure S38. X-ray Microdiffraction data for ROY on phlogopite. Lower traces are simulated powder patterns calculated from the single crystal structures for relevant polymorphs. Gray traces indicate data acquired by secondary integration of portions of the full two-dimensional frame. Secondary integrations were necessary to avoid the regions of strong signal from the crystalline substrates.

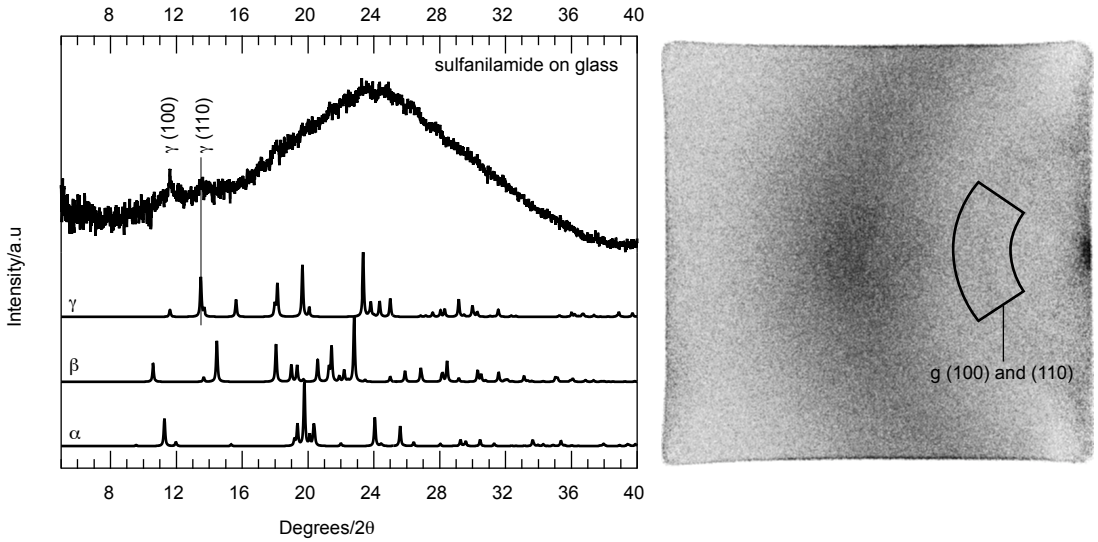

Figure S39. X-ray Microdiffraction data for sulfanilamide on glass. Lower traces are simulated powder patterns calculated from the single crystal structures for relevant polymorphs. Gray traces indicate data acquired by secondary integration of portions of the full two-dimensional frame. Secondary integrations were necessary to avoid the regions of strong signal from the crystalline substrates.

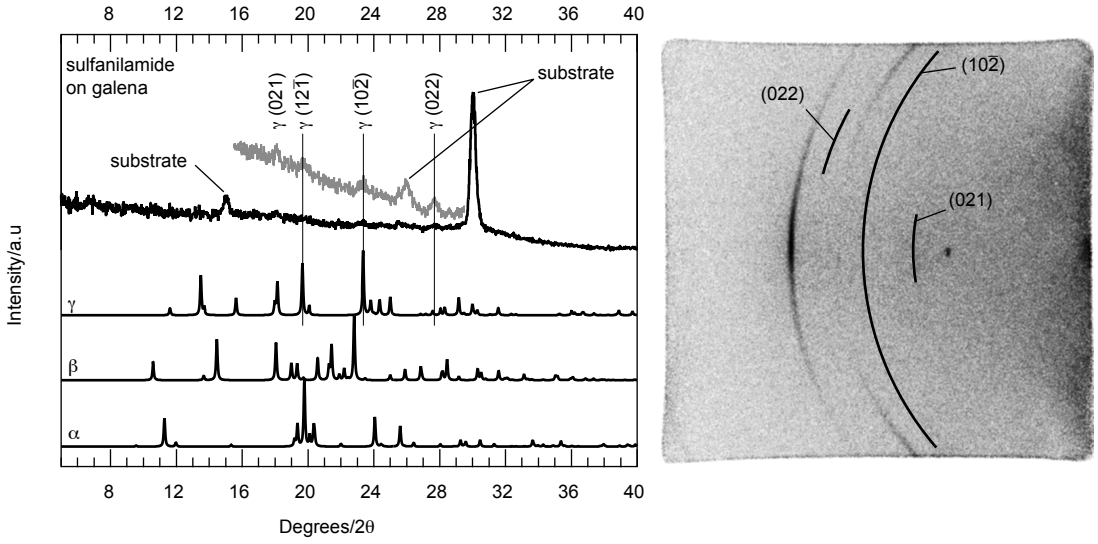

Figure S40. X-ray Microdiffraction data for sulfanilamide on galena. Lower traces are simulated powder patterns calculated from the single crystal structures for relevant polymorphs. Gray traces indicate data acquired by secondary integration of portions of the full two-dimensional frame. Secondary integrations were necessary to avoid the regions of strong signal from the crystalline substrates.

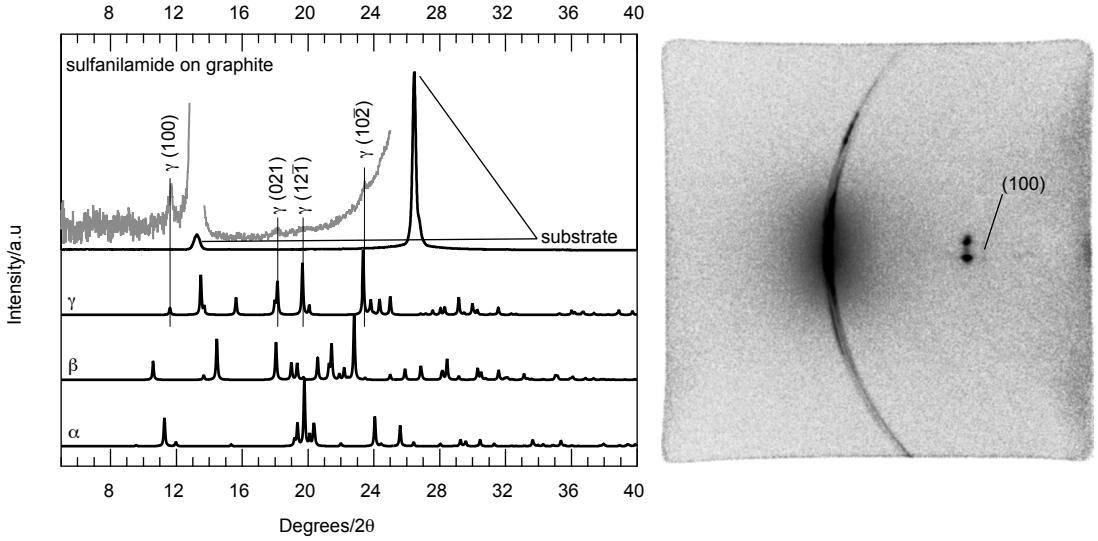

Figure S41. X-ray Microdiffraction data for sulfanilamide on HOPG. Lower traces are simulated powder patterns calculated from the single crystal structures for relevant polymorphs. Gray traces indicate data acquired by secondary integration of portions of the full two-dimensional frame. Secondary integrations were necessary to avoid the regions of strong signal from the crystalline substrates.

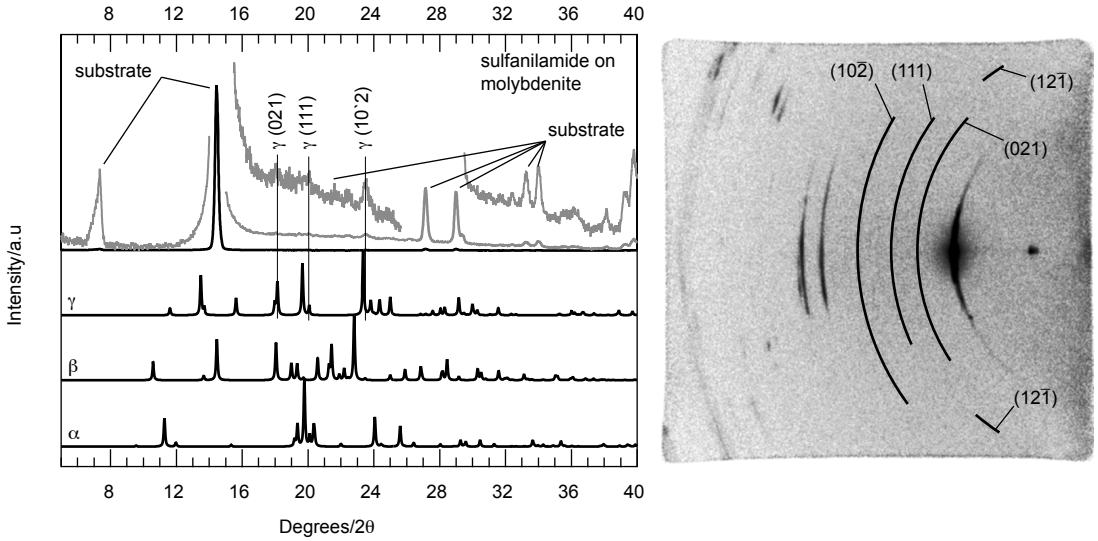

Figure S42. X-ray Microdiffraction data for sulfanilamide on molybdenite. Lower traces are simulated powder patterns calculated from the single crystal structures for relevant polymorphs. Gray traces indicate data acquired by secondary integration of portions of the full two-dimensional frame. Secondary integrations were necessary to avoid the regions of strong signal from the crystalline substrates.

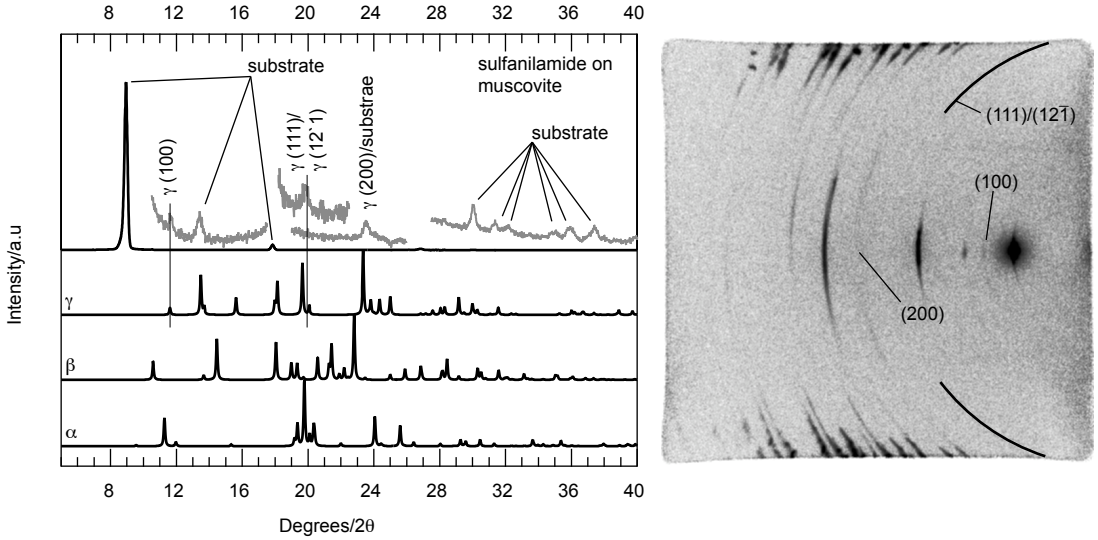

Figure S43. X-ray Microdiffraction data for sulfanilamide on muscovite. Lower traces are simulated powder patterns calculated from the single crystal structures for relevant polymorphs. Gray traces indicate data acquired by secondary integration of portions of the full two-dimensional frame. Secondary integrations were necessary to avoid the regions of strong signal from the crystalline substrates.

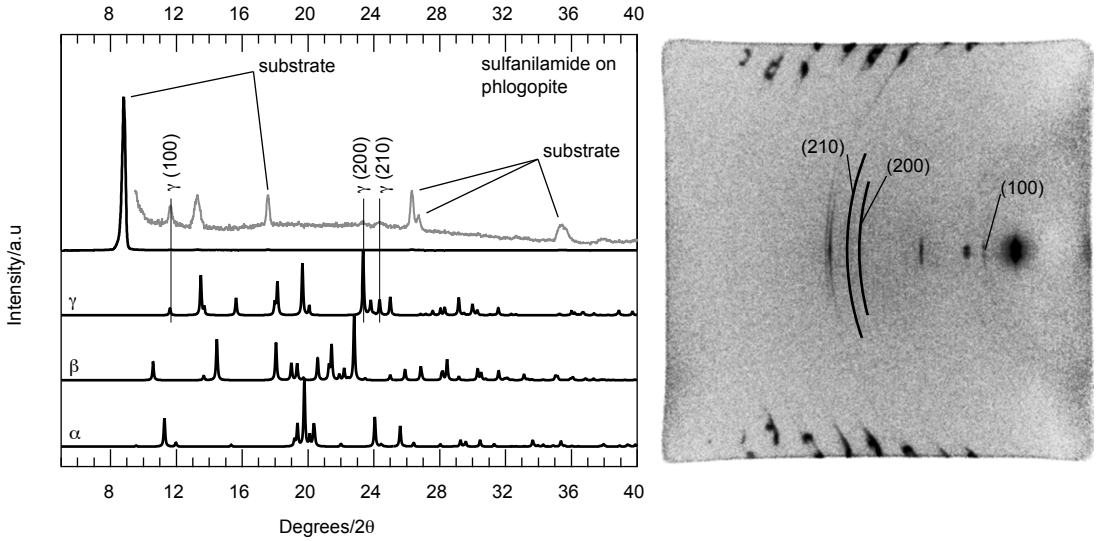

Figure S44. X-ray Microdiffraction data for sulfanilamide on phlogopite. Lower traces are simulated powder patterns calculated from the single crystal structures for relevant polymorphs. Gray traces indicate data acquired by secondary integration of portions of the full two-dimensional frame. Secondary integrations were necessary to avoid the regions of strong signal from the crystalline substrates.

Table S1. Crystallographic data from single crystal structures obtained from the Cambridge Crystallographic Data Centre (CCDC) for polymorphic compounds studied.

	Space group	a/Å	b/Å	c/Å	α/deg	β/deg	γ/deg	Cell vol./Å^3
***Trans*-cinnamic acid**								
α	$P2_1/c$	5.644	18.011	9.019	90	121.47	90	781.967
β	$P2_1/a$	31.296	4.0152	6.083	90	90.146	90	764.385
Glycine								
α	$P2_1/n$	5.0835	11.82	5.4579	90	111.95	90	304.176
β	$P2_1$	5.077	6.268	5.38	90	113.2	90	157.361
γ	$P3_2$	7.046	7.046	5.491	90	90	120	236.084
ROY								
Y	$P2_1/n$	8.5001	16.413	8.5371	90	91.767	90	1190.46
ON	$P2_1/c$	3.9453	18.685	16.3948	90	93.83	90	1205.89
R	$P\bar{1}$	7.4918	7.7902	11.911	75.494	77.806	63.617	598.885
OP	$P2_1/n$	7.976	13.319	11.676	90	104.683	90	1199.86
YN	$P\bar{1}$	4.5918	11.249	12.315	71.194	89.852	88.174	601.825
ORP	Pbca	13.177	8.0209	22.801	90	90	90	2409.87
YT04	$P2_1/n$	8.2324	11.8173	12.3121	90	102.505	90	1169.36
Sulfanilamide								
α	Pbca	5.65	18.509	14.794	90	90	90	304.176
β	$P2_1/c$	8.975	9.005	10.039	90	111.43	90	157.361
γ	$P2_1/c$	7.95	12.945	7.79	90	106.5	90	236.084

Table S2. Two-dimensional lattice parameters for the cleavage planes of substrates studied. Data acquired from the Inorganic Crystal Structural Database (ICSD).

	a_1/Å	a_2/Å	α/deg.
Galena	5.936	5.936	90
HOPG	2.4612	2.4612	120
Molybdenite	3.1604	3.1604	120
Muscovite	5.203	8.995	90
Phlogopite	5.326	9.210	90

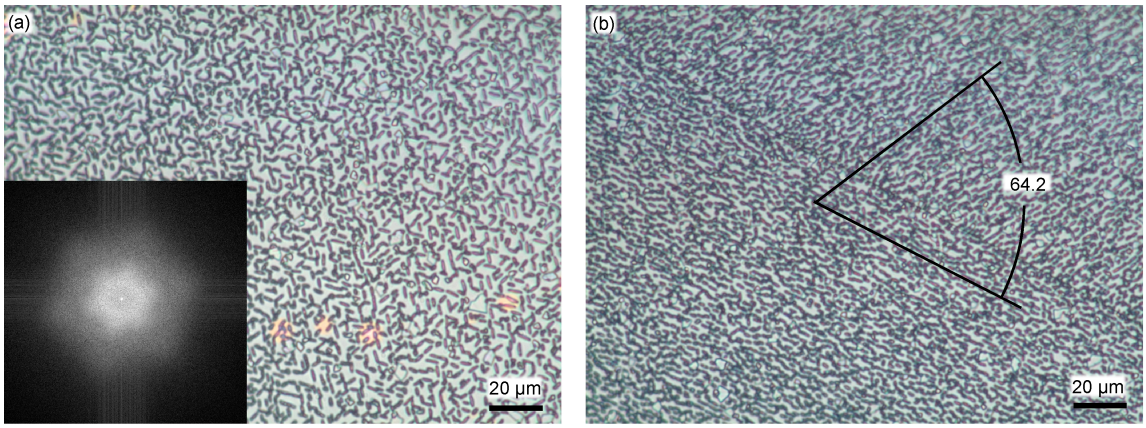

Figure S45. Enlargement of **Figure 5** from the manuscript.